NEURAL DYNAMICS OF VISUAL MOTION PERCEPTION:
LOCAL DETECTION AND GLOBAL GROUPING

Stephen Grossberg† and Ennio Mingolla‡

Center for Adaptive Systems
and
Department of Cognitive and Neural Systems
Boston University
111 Cummington Street
Boston, Massachusetts 02215

Abstract

How do we perceive coherent patterns of motion in regions of our visual fields containing distributions of locally ambiguous motion signals? How does the visual system solve the twin problems of segmentation, the segregation of motion signals from nearby signals belonging to other objects with different trajectories, and grouping, the combining of relatively distant or separated and often locally unequal motion signals into coherent perceptual objects? A neural network model of global motion segmentation and grouping by visual cortex is here described. Called the Motion Boundary Contour System (BCS), the model clarifies how ambiguous local movements on a complex moving shape are actively reorganized into a coherent global motion signal. Unlike many previous researchers, we analyse how a coherent motion signal is imparted to all regions of a moving figure, not only to regions at which unambiguous motion signals exist. The model hereby suggests a solution to the global aperture problem. The Motion BCS describes how preprocessing of motion signals by a Motion Oriented Contrast Filter (MOC Filter) is joined to long-range cooperative grouping mechanisms in a Motion Cooperative-Competitive Loop (MOCC Loop) to control phenomena such as motion capture. The Motion BCS is computed in parallel with the Static BCS of Grossberg and Mingolla (1985a, 1985b, 1987). Homologous properties of the Motion BCS and the Static BCS, specialized to process movement directions and static orientations, respectively, support a unified explanation of many data about static form perception and motion form perception that have heretofore been unexplained or treated separately. It is shown how the Motion BCS can compute motion directions that may be synthesized from multiple orientations with opposite directions-of-contrast. Interactions of model simple cells, complex cells, hypercomplex cells, and bipole cells are described, with special emphasis given to new functional roles in direction disambiguation for end stopping at multiple processing stages and to the dynamic interplay of spatially short-range and long-range interactions.

1. Introduction: The Aperture Problem and Motion Grouping

The unity and persistent identity of objects undergoing motion is so immediate that we may all too readily take for granted the subtle problems posed in discriminating such unity within the scintillating mosaic of visual stimulation. In the familiar example of trying to detect a leopard moving through a forest canopy, the change in the optic array over time is a jumble of contrast changes whose local components point in a variety of directions, due to the vagaries of the motions of rustling leaves and of the occlusions and disocclusions of markings on the leopard's body. For a leopard to be detected in such contexts, a key problem must be solved: How can the locally ambiguous local motion signals corresponding to the many parts of the leopard's body be *reorganized* into a coherent object whole with a unitary motion?

The *aperture problem* illustrates these issues in a vivid way. It inquires into how a straight edge or grating viewed through a circular aperture appears to be moving perpendicular to its orientation of contrast regardless of its true motion direction (Wallach, 1976). While this description of the aperture problem is at the molar perceptual level, any early visual cell with a localized receptive field, whether concentric or elongated, experiences its own "aperture problem," because its estimate of motion direction is a spatiotemporally weighted function of changes in local stimulation only. Adelson and Movshon (1982) introduced diagrams similar to Figure 1a to illustrate the ambiguity of local motion direction and speed from information confined to an aperture. In this figure, the length of arrows codes possible trajectories of the point A that would be consistent with the measured change of contrast over time of the cell in question. These authors use the term "velocity space" to emphasize that such a cell seems to be sensitive to the normal component of velocity. A complementary way of thinking about this situation is illustrated in Figure 1b, in which the length of arrows is roughly proportional to the cell's "prior probability distribution" for interpreting changing stimulation as occurring in one of several directions. The direction perpendicular to the cell's receptive field's orientation is locally preferred. However, a cell with an oriented receptive field, such as a simple cell, may be stimulated by a moving edge that is not perfectly aligned with its receptive field's dark-to-light contrast axis. Within a hypercolumn of cells that are tuned to similar position, spatial frequency, contrast, and temporal parameters but vary in preferred orientation (Hubel and Wiesel, 1977), the distribution of local motion signals across cells tuned to all orientations at a given position would favor the direction perpendicular to the orientation of the edge.

The barberpole illusion (Wallach, 1976) shows that these local preferences can be readily overridden by global factors related to the forms within which stationary and moving segments of a display are located (Figure 2). This illusion indicates that, to the extent that locally *unambiguous* motion signals exist at line ends or corners, those unambiguous signals can somehow enforce an interpretation of motion direction consistent with their own throughout the length of a contour bounded by those ends or corners (Figure 3). Clearly some long-range grouping process subsequent to the early generation of local motion signals is at work. This process acts to cooperatively "choose and sharpen" relatively large domains of ambiguous signals using relatively localized, but unambiguous, signals.

In a recent psychophysical study of motion perception, Mingolla, Todd, and Norman (1992) created displays containing spatial arrays of many small circular apertures. For each display, a single "true" motion underlying the trajectories of all visible elements was
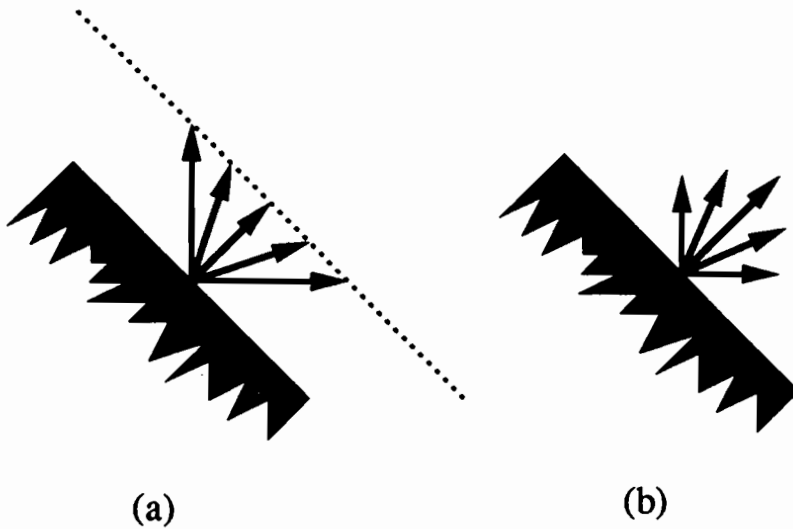
(a)   (b)

Figure 1: (a) This "velocity space" construction, adapted from Adelson and Movshon (1982), illustrates that the motion of a given point on a moving edge could be along any of the trajectories whose arrows end on the dashed line. (b) A complementary way to view this direction ambiguity is to consider that local motion signals from a straight edge are *strongest* in the perpendicular direction, while covering a range of possible directions.

defined, and the nature and juxtaposition of those elements was manipulated in order to investigate the nature of perceptual grouping of motion signals in a direction discrimination task. The apertures at times contained only straight lines extending to the circumference of the aperture, as in the classical description of the aperture problem, and at other times contained line ends or intersections that provided potential information concerning the "true" motion of the display. The results of the experiments revealed a strong tendency of the visual system to form some kind of average of information in the local motion signals derived from oriented straight contours, as displayed in Figure 1b, if that was the only kind of information present. The addition of identifiable features whose trajectories could be tracked over time affected direction discrimination in in complex way, however. At times featural trajectories were prepotent, completely determining a subject's perceived direction, while at other times a compromise between the trajectories supported by the featural information and those supported by the averaging process appeared to be struck.

The results of Mingolla, Todd, and Norman (1992) illustrate the dynamic nature of the processes whereby the visual system combines a diverse set of local motion signals that "belong" to the same object and separate them from similar sets of signals taken to come
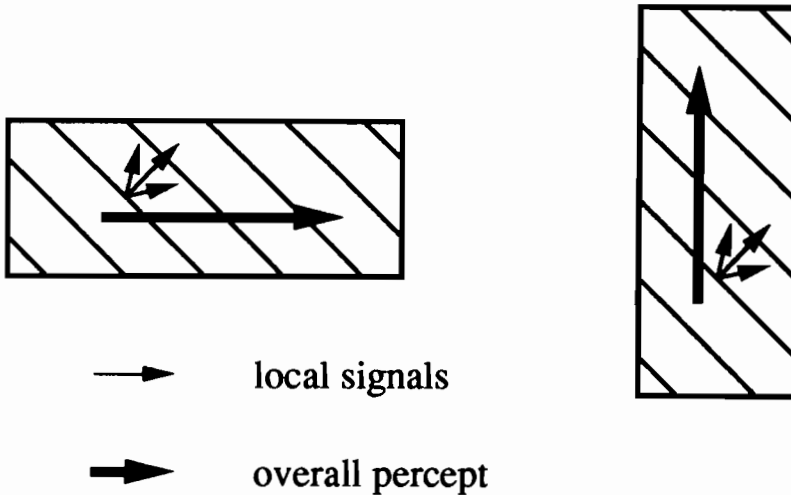
Figure 2: In the barberpole illusion a striped pattern is perceived as moving in the direction of elongation of a rectangular frame (or aperture). Local motion signals, indicated in by thin arrows at only one location within each rectangle, are generated throughout the interior lengths of each diagonal line. As indicated in Figure 1b, these local motion signals express both ambiguity and preference regarding direction of motion. Despite the large area covered by the ambiguous and diagonal-motion-preferring local signals, the resulting percept is horizontal or vertical, depending on the configuration of a visible frame (or aperture).

from different neighboring (segmentation) or overlapping (transparency) objects. Our theory introduces processes that clarify how such grouping effects are generated both during motion perception and the perception of static form.

    Some of the subtle issues about grouping that occur during static form perception are illustrated in Figure 4. As pointed out by Prazdny (1984), reversing the contrast relative to a neutral background of one set of dots in a Glass pattern can weaken, or even annihilate, the grouping percept (Figures 4a and 4b). The paradoxical nature of this result can best be appreciated by juxtaposing it with the striking illusory groupings that can be sustained between the like directions-of-contrast (Figure 4c) of the Kanizsa square, as well as the opposite directions-of-contrast (Figure 4d) of the "reverse contrast Kanizsa square" (Cohen and Grossberg, 1984; Grossberg and Mingolla, 1985b; Prazdny, 1984; Shapley and Gordon, 1985). A similar pattern of sensitivity to direction-of-contrast at short-range and insensitivity to direction-of-contrast at long-range also occurs in motion perception. For "short-range" motion, reversal of dot contrast between frames of random dot cinematograms abolishes
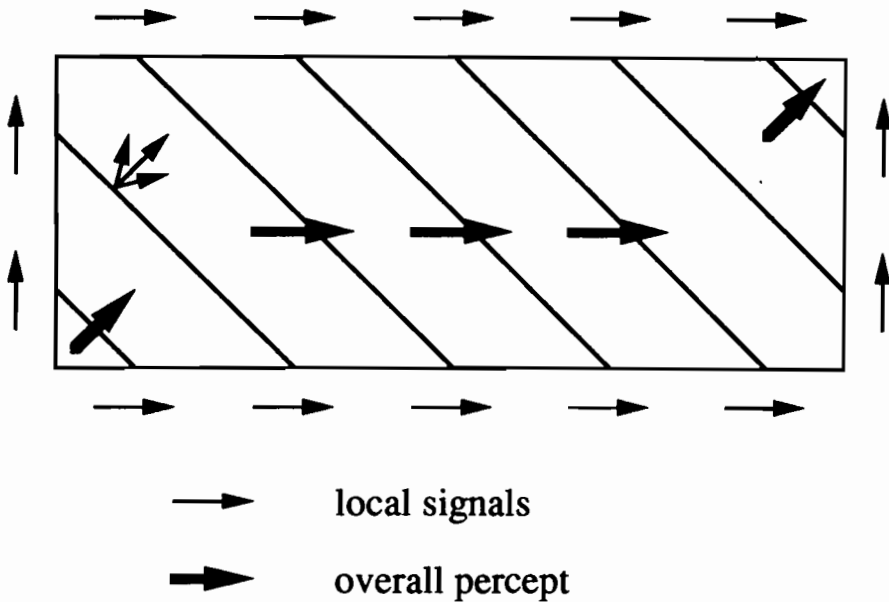
local signals

overall percept

Figure 3: A closer look at the barberpole illusion reveals that for sufficiently large displays, whose length-to-width ratio is not too far from unity, the overall motion percept may vary across different areas of the display. The perceived motion near the lower left and upper right corners of the rectangle may be diagonal, while horizontal motion is seen through the bulk of the display. Unambiguous motion signals are generated in the region where each diagonal line meets the horizontal and vertical contours of the rectangle. (These unambiguous signals are diagramed *outside* the rectangle for clarity.) Evidently, such unambiguous signals exert an influence on the percept that is disproportionate to their areal extent, since the overall percept throughout a diagonal line tends to be a resultant (horizontal plus vertical to diagonal or horizontal plus horizontal to horizontal) of those signals.

a coherent motion percept, whereas long-range apparent motion can occur using displays whose contrast with respect to the background reverses between frames (Anstis and Mather, 1985). These different grouping effects are explained within the theory that is reviewed below.

2. The Static and Motion Boundary Contour Systems

The central theme of our modeling work is thus the investigation of mechanisms whereby an array of locally ambiguous motion signals can be globally reorganized into coherent object motion signals. Our investigation of the global reorganization of local motion signals is conducted within a theoretical framework which has already analysed analogous problems
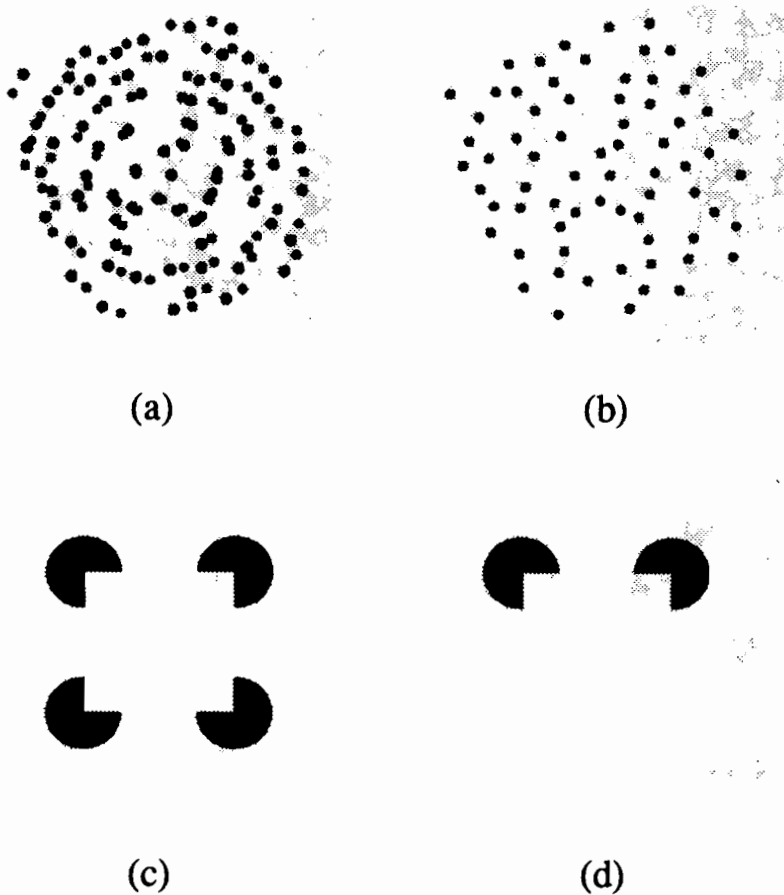
Figure 4: The subtleties of the interaction of spatial scale and direction-of-contrast are revealed by the juxtposition of two classical visual phenomena. Parts (a) and (b) illustrate how the formation of Glass patterns is destroyed by reversing the contrast of one field of dots (Prazdny, 1984), while the reversal of contrast of inducers in the Kanizsa square configuration from (c) to (d) does not significantly weaken illusory contour formation.

within the domain of static form perception. This latter theory has been called FACADE Theory, because its visual representations are predicted to multiplex together properties of Form-And-Color-And-DEpth in prestriate cortical area V4. FACADE Theory describes the neural architecture of two subsystems, the Boundary Contour System (BCS) and the Feature Contour System (FCS), whose properties are computationally complementary (Grossberg, Mingolla, and Todorović, 1989). The BCS generates an emergent 3-D boundary segmentation of edges, texture, shading, and stereo information at multiple spatial scales (Grossberg, 1987a, 1987b, 1990; Grossberg and Marshall, 1989; Grossberg and Mingolla, 1985a, 1985b,

1987). The FCS compensates for variable illumination conditions and fills-in surface properties of brightness, color, and depth among multiple spatial scales (Cohen and Grossberg, 1984; Grossberg, 1987a, 1987b; Grossberg and Mingolla, 1985a; Grossberg and Todorović, 1988).

The BCS provided a new computational rationale as well as a model of the neural circuits governing classical cortical cell types such as simple cells, complex cells, and hypercomplex cells in cortical areas V1 and V2. The theory also predicted a new cell type, the bipole cell (Cohen and Grossberg, 1984; Grossberg and Mingolla, 1985a) whose properties have been supported by neurophysiological experiments (von der Heydt, Peterhans, and Baumgartner, 1984; Peterhans and von der Heydt, 1989). Many heretofore unexplained phenomena about the perception of Form-And-Color-And-Depth have been clarified by FACADE Theory, and an ever increasing number of laboratories have been carrying out experiments suggested by its concepts and mechanisms (Eskew *et al.*, 1991; Humphreys, Quinlan, and Riddoch, 1989; Kellman and Shipley, 1991; Meyer and Dougherty, 1987; Mikaelian, Linton, and Phillips, 1990; Paradiso and Nakayama, 1991; Peterhans and von der Heydt, 1989; Prinzmetal, 1990; Prinzmetal and Boaz, 1989; Sutter, Beck, and Graham, 1989; Todd and Akerstrom, 1987; Watanabe and Sato, 1989; Watanabe and Takeichi, 1990).

This BCS model, now called the *Static* BCS model, consists of several parallel copies, such that each copy is activated by a different range of receptive field sizes. Each Static BCS copy is further subdivided into two hierarchically organized systems (Figure 5): a *Static Oriented Contrast Filter*, or *SOC Filter*, for preprocessing quasi-static images (the eye never ceases to jiggle in its orbit); and a Cooperative-Competitive Feedback Loop, or CC Loop, for generating coherent emergent boundary segmentations of the filtered signals.

After the development of the Static BCS reached a certain level of clarity, it focused attention on the perplexing question: How do static and motion perception systems differ? Some regions of visual cortex are specialized for motion processing, notably region MT (Albright, Desimone, and Gross, 1984; Maunsell and van Essen, 1983; Newsome, Gizzi, and Movshon, 1983; Zeki, 1974a, 1974b). However, even the earliest stages of visual cortical processing, such as simple cells in V1, require stimuli that change through time for their maximal activation and are direction-sensitive (DeValois, Albrecht, and Thorell, 1982; Heggelund, 1981; Hubel and Wiesel, 1962, 1968, 1977; Tanaka, Lee, and Creutzfeldt, 1983). Why has evolution generated regions such as MT, when even V1 is change-sensitive and direction-sensitive? What computational properties are achieved by the $V1 \rightarrow MT$ cortical stream that cannot be achieved by the parallel $V1 \rightarrow V2 \rightarrow V4$ cortical stream?

Analysis of the SOC Filter design revealed that one of its basic properties made it unsuitable for motion processing. In particular, SOC Filter output signals cannot adequately discriminate the direction-of-motion of a moving figure. Further analysis of how this happens and how it can be overcome led to a new theory of biological motion perception that was outlined in Grossberg (1987b) and quantitatively specified and analysed in Grossberg (1990, 1991) and Grossberg and Rudd (1989a, 1989b, 1992). The results of this analysis suggested that the motion form perception system shares many design features with the static form perception system, but that it has incorporated the minimal changes needed to achieve sensitivity to both local and global properties of direction-of-motion. In fact, Grossberg (1990, 1991) has suggested that the two systems are parallel subsystems of a larger, symmetric system design, called Form-Motion (FM) Symmetry, that is predicted to govern the devel-
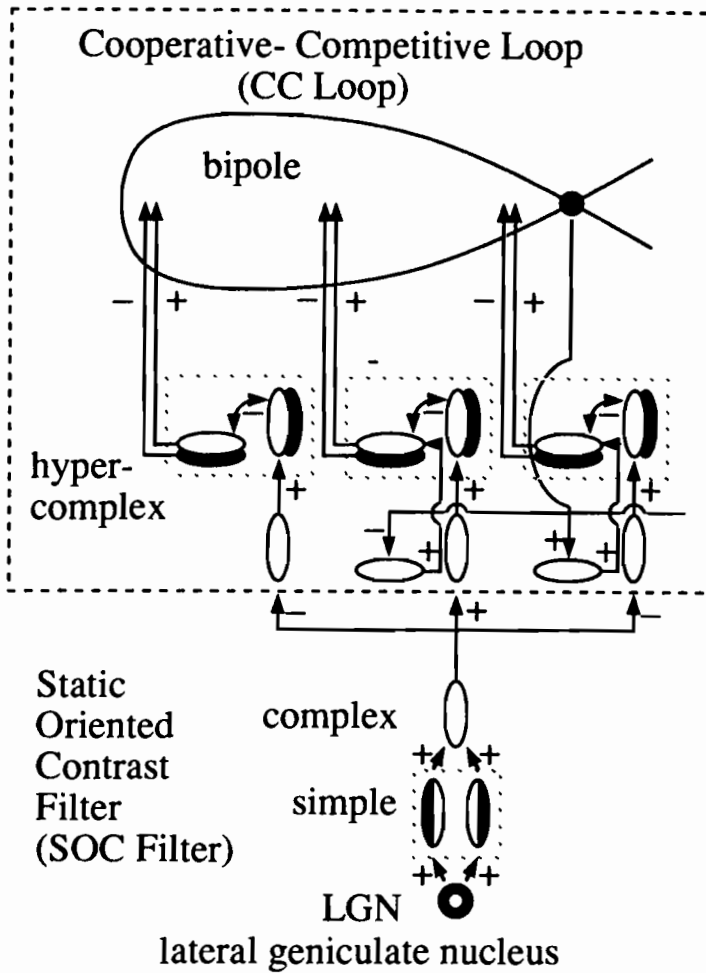
Figure 5: The static Boundary contour system consists of two main parts, the Static Oriented Contrast Filter (SOC Filter) and the Cooperative-Competitive Loop (CC Loop). The SOC Filter determines the locally preferred orientations of contrast differences in the input, while the CC Loop groups, selects, and sharpens contours, both "real" and "illusory."

opment of visual cortex. See Grossberg (this volume) for a discussion of FM Symmetry and the differences between the Static BCS and Motion BCS.

Correspondingly, this new theory of biological motion perception consists of a neural architecture called a *Motion Boundary Contour System*, or *Motion BCS*. The Motion BCS consists of several parallel copies, such that each copy is activated by a different range of receptive field sizes, as in the Static BCS. Also as in the Static BCS, each Motion BCS copy is

further subdivided into hierarchically organized subsystems: a *Motion Oriented Contrast Filter*, or *MOC Filter*, for preprocessing moving images; and a Motion Cooperative-Competitive Feedback Loop, or MOCC Loop, for generating coherent emergent boundary segmentations of the filtered signals. The MOC Filter provides a model for the early stages of the $V1 \rightarrow MT$ processing stream in the visual cortex. Evidence for the MOC Filter includes its ability to explain many classical and recent data about short-range and long-range motion properties, and about cortical cell properties, that have not yet been explained by alternative models. Grossberg and Rudd (1989a) have also shown how properties of other motion perception models can be assimilated into different parts of the Motion BCS design.

The computer simulations of motion perception data that were reported by Grossberg and Rudd (1989a, 1989b, 1992) used a 1-dimensional version of the MOC Filter. The present article simulates data which require a 2-dimensional version of the MOC Filter. In addition, outputs from the 2-dimensional MOC filter input to a 2-dimensional version of the MOCC Loop. In order to motivate these results, we first discuss key motion segmentation and grouping phenomena, including the aperture problem, barberpole illusion, and motion capture. Then we discuss how these phenomena suggest the existence of a MOCC Loop which is analogous to the static CC Loop of Grossberg and Mingolla (1985a, 1985b, 1987) but is specialized to process moving images. The MOC Filter of Grossberg and Rudd (1989a, 1992) is reviewed in Grossberg (this volume). In this chapter, we show how the MOC Filter model can be extended to process 2-dimensional moving images. These extensions include hypotheses concerning the role of end-stopped simple cells, the spatial layout of simple cell receptive fields, and competition among signals sensitive to different directions-of-motion. We illustrate these concepts through computer simulations which study how the Motion BCS responds to changes in the bounding orientations, shapes, and motion directions of an object. These results are used to explain data about the aperture problem, barberpole illusion, and motion capture.

3. Global Segmentation and Grouping: From Locally Ambiguous Motion Signals to Coherent Object Motion Signals

As described in the previous section, the barberpole illusion (Figures 2 and 3) offers compelling evidence for long range cooperative processes in motion perception. Cooperativity among motion signals was studied by Lappin and Bell (1976) and more recently by Williams and Sekuler (1984). Random dot cinematograms were displayed in which successive displacements of dots over frames were not uniform across all dots, but rather were sampled from a rectangular distribution of possible directions. On any frame each dot's displacement was independent of both its own history of displacements and of the displacement of other dots in that frame. For appropriate parameter choices, observers reported perceiving a coherent global motion in the direction of the mean of sampled local dot motions, as well as perceiving the individual motions of each dot. Williams and Sekuler also reported hysteresis effects, whereby the percept of coherent motion persisted while motion distribution parameters were altered from a relatively narrow range, which easily supported the coherent percept, to a wider range, for which coherent motion was not ordinarily seen if presented initially. Thus cooperativity among motion signals involves averaging of directional information and hysteresis, as well as sharpening and choice.

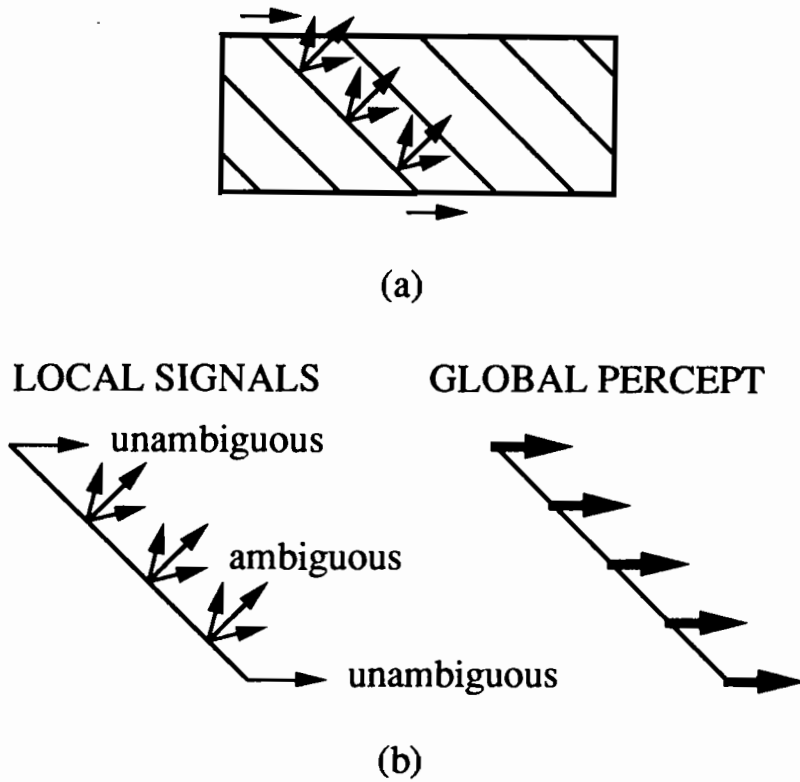Ramachandran (1981) and Ramachandran and Inada (1985) provided additional evi-

(a)

(b)

Figure 6: (a) By focusing on the distribution of motion signals on a single diagonal line, as indicated in the barberpole illusion, the phenomenon can be analysed as a form of motion capture. (b) The unambiguous signals from the line ends help to enhance signals of like direction (cooperation) and suppress signals of different directions (competition) within the interior of the line segment.

dence for cooperation among motion signals in a phenomena termed "motion capture," in which strong and unambiguous motion signals can actively reorganize motion signals in ambiguous regions where there are no locally preferred motion directions. From this perspective, the barberpole illusion can be analysed as displaying its own form of "motion capture," as indicated in Figure 6. That is, signals from the ambiguous interior region of the diagonal line segment are being "captured" by signals from the unambiguous ends. This enhancement of horizontal signals in the interior region is accompanied by the suppression of diagonal and vertical signals. Long-range cooperation is thus accompanied by short-range competition in order to enforce a clear choice of percept all along the line. As noted below, this cooperative-competitive interaction is analogous to that of the Static CC Loop.

bipole:

similar orientations

COOPERATE

+   +   +

−

hypercomplex

COMPETE

with less favored orientations

Figure 7: In the static cooperative-competitive feedback loop (CC Loop) signals of like orientation (here horizontal) initiated from "bottom up" input data arrive at two locations separated by some distance (indicated by the horizontal bar above the word "hypercomplex" and the corresponding bar at the lower right). Cooperative bipole cells, identified with projections of V2 cells, can, if they receive sufficient stimulation on *both* sides of their receptive field centers, send positive feedback to cells of like orientation in the hypercomplex layer. There cells of differing orientation and like position compete with each other to determine the most favorable orientation at each location. Because of the long-range feedback, local orientational preferences are modulated to be consistent with contextual data. While in this example, the completion is colinear, the "figure eight" shape of the bipole cell indicates that completion can be curvilinear, so long as a consistent co-occurrence of oriented signals favors interpolation at the bipole center. See Figure 28 and equations (A13) through (A21) of the Appendix of Grossberg and Mingolla (1985b) for a detailed explanation of static bipole cells.

4. Coherent and Resonant Completion: Static and Motion CC Loops

Static BCS mechanisms also combine long-range cooperation with short-range competition among orientationally tuned cells within a feedback network, namely the CC Loop (Figure 7). Since publication of the CC Loop equations in Grossberg and Mingolla (1985a, 1985b, 1987), increasing physiological evidence for the model has been reported. In particular, Peterhans and von der Heydt (1989) have recently reported evidence for cooperative

linking interactions in cortical area V2, and Gray *et al.* (1989) and Eckhorn *et al.* (1988) have reported resonant interactions involving phase locking of spike trains of V2 cells with nonoverlapping receptive fields, which also occurs due to the long-range cooperative interactions of the CC Loop (Grossberg and Somers, 1991).

Given that the Static CC Loop can enhance consistent signals and suppress inconsistent or ambiguous signals from orientationally-tuned cells, and given that *in vivo* early orientationally tuned cells, such as simple cells, are sensitive to motion, the question naturally arose whether motion segmentation could be accomplished by the Static CC Loop. Our daily experiences with the dynamic geometry of form perception for static and moving contours suggests that this is not true. As illustrated in Figure 8, a *static* form system is concerned with *orientation* of contours, while a *motion* form system is concerned with *direction* of moving contours. Moreover, these systems must be different because the geometries governing static orientations and motion directions are different. For example, the opposite orientation of "vertical" is "horizontal," a difference of 90°, whereas the opposite direction of "up" is "down," a difference of 180°. Grossberg (1991, this volume) has suggested an explanation of this difference. Keeping track of direction as well as orientation requires an additional degree of freedom, since a segment of a given orientation may be moving in any of several directions, and a given direction of motion can be observed for segments of any of several orientations. This is just another way of stating the aperture problem.

The striking similarity of cooperative and competitive grouping requirements for both static and moving images, together with the existence of different geometries for static and motion perception, suggested that parallel versions of the CC Loop exist within a Static BCS and a Motion BCS. Additional analyses of short-range and long-range motion data suggested, moreover, that parallel versions of OC Filters exist within the Static BCS and the Motion BCS (Grossberg and Rudd, 1989a, 1992). This taxonomy of "static" and "motion" CC Loops does not, however, imply logical exclusivity of function. When a contour moves, the *static* CC Loop may operate to determine the best coherent *orientations* of the moving contour, at the same time that the *motion* CC Loop determines the best coherent *directions* of that contour. Moreover, the orientationally-based boundary segmentations that are generated by the Static BCS are suggested to help select directionally-based boundary segmentations of the Motion BCS at correctly calibrated depths (Grossberg, 1991, this volume). This interaction has been predicted to occur via the $V1 \to V2 \to MT$ pathway.

5. Many Orientations Can Move in the Same Direction

How then do the motion analogs of the cooperative bipole cells (Figure 7) of the static CC Loop function? In analysing the properties of static bipole cells, certain images by John Kennedy proved invaluable (Kennedy, 1979). As shown in Figure 9, static bipole cells are capable of choosing orientations which are not locally preferred for generating positive feedback to cooperatively link and complete static boundaries. Each bipole cell can generate an output signal only if *both* of its oriented receptive fields receive large enough inputs from cells with similarly oriented receptive fields. These input cells at the previous processing level consist of formal analogs of hypercomplex cells. The output signals from the bipole cells feed back to the hypercomplex cells (Figure 7), where they bias the competition among the hypercomplex cells towards the orientations and positions that are most favored by the bipole cells.
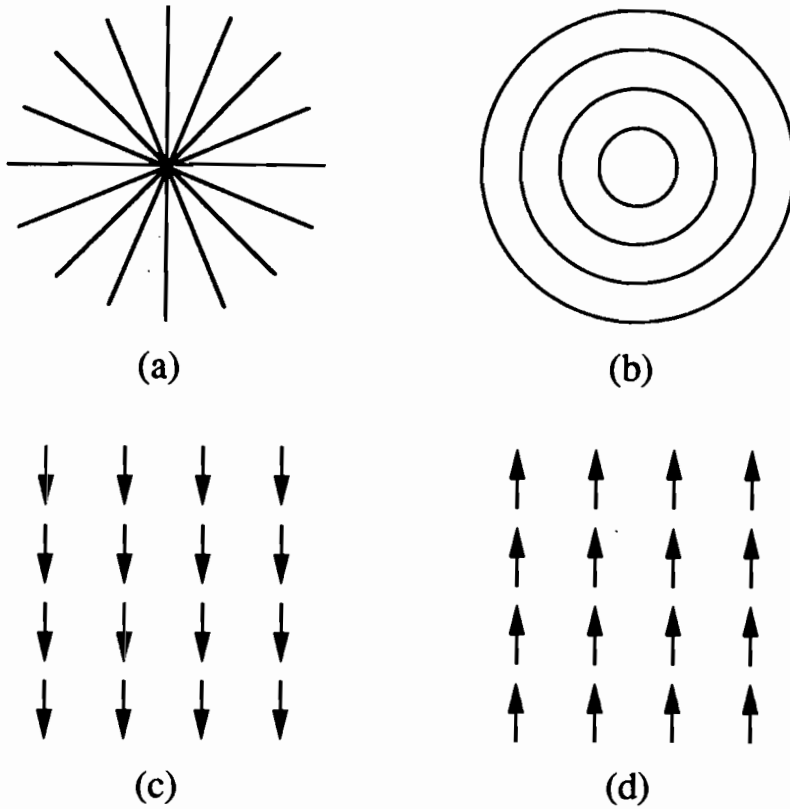
(a)   (b)

(c)   (d)

Figure 8: As indicated by such static rebound phenomena as the Mackay effect, in which prolonged fixation on a pattern of radial line segments (a) results in an aftereffect of perceived circular contours (b), the opposite of an static *orientation* signal is a signal of perpendicular orientation. The waterfall illusion, in which prolonged adaptation to motion signals as from a waterfall (c) is followed by the sensation of upward motion when one looks at a neutral scene (d), indicates that the opposite of a motion *direction* signal is not 90° but 180° from that signal.

The Motion CC, or MOCC, Loop must, however, cope with an additional degree of freedom, since it considers direction as well as orientation. Thus motion bipole cells are organized in a fashion that differs somewhat from that of their static analogs. As indicated in Figure 10, motion bipole cells are postulated to exist in families sensitive to motion signals of different directions but whose sources are arrayed in patterns of similar orientation. Expressed differently, while some motion bipole cells are assumed to favor the direction of motion perpendicular to the orientation induced by the elongated axis of their two lobes
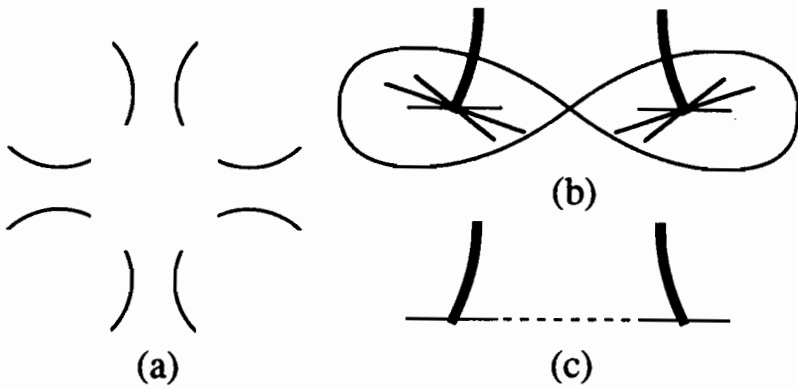
Figure 9: (a) This illusory contour display, adapted with permission from Kennedy (1979), indicates that boundary completion in the static CC Loop can choose orientations that are not locally preferred if global organizational factors are sufficiently powerful. (b) The locally preferred directions at the bottom ends of the two top curves of (a) are perpendicular to the ends of the curves and thus tilted off the horizontal. (c) Cooperation among signals that are horizontal enhances and completes horizontal signals (cooperation) while suppressing non-horizontal signals (competition) along the illusory contour.

(Figure 10b), others have a similar spatial layout but different preferred directions of motion (Figure 10a and 10c).

As in the Static CC Loop, each bipole cell of the MOCC Loop can generate an output signal only if *both* of its receptive fields receive large enough inputs from cells that are sensitive to a similar direction-of-motion. These input cells at the previous processing level consist of formal analogs of hypercomplex cells. The output signals from the bipole cells feed back to the hypercomplex cells, where they bias the competition among the hypercomplex cells towards the directions and positions that are most favored by the bipole cells.

It is intuitively clear that this is just the sort of cooperative feedback, propagated inward between pairs, or larger numbers, of flanking inducers, that is needed to explain phenomena like the barberpole illusion and motion capture. Our analysis elevates this intuition into a computationally precise theory. As a result, both orientationally-sensitive grouping during static form perception and directionally-sensitive grouping during motion form perception are predicted to utilize bipole cells. The explanatory power of this homology strengthens the case that both the Static BCS and Motion BCS architectures are variations of a common cortical design.

(a)   (b)   (c)
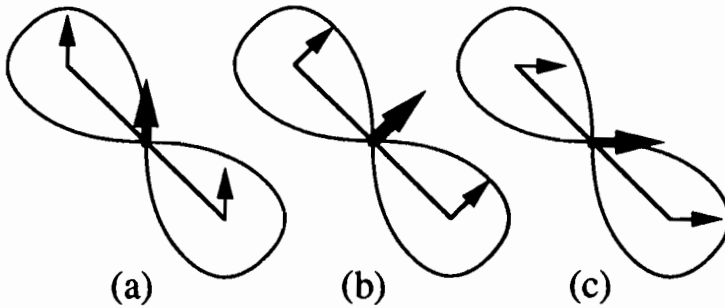
Figure 10: As with static bipole cells, motion bipoles are sensitive to bottom-up direction signals from motion hypercomplex cells (indicated by thin arrows), which send excitatory signals to each lobe of the bipole cell. If sufficient excitatory activity is sensed in *both* lobes, the bipole sends feedback signals of like direction (indicated by thick arrows) to the hypercomplex layer. While analogous to their static counterparts, motion bipole cells fundamentally different, insofar as they must cope with the additional degree of freedom imposed by the simultaneous determination of a globally consistent motion direction over many possible contour orientations. Thus families of bipole cells are presumed to exist, such that cells whose major axes are the same (diagonal in the present case) can be maximally sensitive to motion signals of different directions, ranging from (a) vertical to (b) diagonal (perpendicular to the major axis) to (c) horizontal for the three bipoles shown here.

6. Joining Sensitivity to Direction-of-Motion with Insensitivity to Direction-of-Contrast

In order to design a MOCC Loop, its hypercomplex cells need to be sensitive to a prescribed direction-of-motion. These cells may be excited by image contours with different orientations all moving in the same direction within a prescribed region of perceptual space. In order to synthesize directional sensitivity from several different orientations, the MOC Filter needs to have a somewhat different circuit design than the SOC Filter. As noted in Grossberg (this volume), the reason for this modification is that complex cells of the SOC Filter are insensitive to direction-of-motion as well as to direction-of-contrast. Consequently, the SOC Filter cannot be used to process the direction-of-motion of a moving figure. This deficiency arises from the way in which the SOC Filter becomes insensitive to direction-of-contrast at its complex cell level.

The main design problem leading to a MOC Filter is to make the minimal changes in the SOC Filter that are needed to model an oriented, contrast-sensitive filter whose outputs are insensitive to direction-of-contrast—a property that is just as important for moving images as for static images—yet is also *sensitive* to direction-of-motion—a property that is certainly essential in a motion perception system. Along the way, the MOC Filter introduces an extra degree of computational freedom which achieves several important properties in one

stroke: sensitivity to direction-of-motion, long-range motion interactions, and binocularity (Grossberg and Rudd, 1989a, 1992).

7. Pooling Orientations and Directions-of-Contrast to Compute 2-D Directions-of-Motion

The Grossberg-Rudd model (Figure 11; see Grossberg, this volume) was used to explain and simulate motion data which exhibit a natural one-dimensional, or 1-D, symmetry; for example, apparent motion between colinear groups of flashes. The model needs further development to explain data concerning the motion of 2-D shapes, since such shapes may move in directions that may or may not be perpendicular to the orientations of their boundaries. The type of new issues that arise in the 2-D case are illustrated by the following example. Consider the lower right corner of a homogeneous rectangular form of relatively high luminance that is moving diagonally upward and to the right on a homogeneous background of relatively low luminance (Figure 12). Both the regions of horizontal and vertical contrast near the corner provide signals to the MOC Filter, provided that the sustained cells of Level 2 are spatially laid out as indicated in Figure 13. Here the direction of motion is diagonal to the orientational preference of the individual sustained cells. These vertically and horizontally oriented cells contribute to the total signal that codes movement in the diagonally upward direction. So too do cells whose orientation is perpendicular to the diagonal direction. On the other hand, cells whose orientation is colinear with the direction of motion should not be included.

Accordingly, each motion detector is assumed to receive weighted inputs from all sustained-transient cells whose orientations differ from the preferred direction-of-motion by no more than 90 degrees, and whose preferred positions lie within a prescribed distance from the preferred position of the motion detector. As indicated in Figure 14, the long range filter (Level 5, Figure 11) can simultaneously accept motion signals from both the horizontal and vertical edges of the moving corner, despite the gating of one set of signals by transient "luminance increasing" on-cells and gating of another set by "luminance decreasing" off-cells (Level 3, Figure 11). Thus while simultaneous increase and decrease of luminance is logically impossible in an infinitesimal area, and while a too rapid change from increase to decrease may be unresolvable by sustained cells at Level 2, the simultaneous increase and decrease of luminance at different orientations and different locations, but in the same direction, are pooled by the long-range filter. This sort of long-range filtering by MOC Filter complex cells is not the same as the still longer-range cooperative grouping by CC Loop bipole cells.

8. Sustained-Transient Gating before Short-Range Spatial Filtering

In attempting to simulate the 2-D MOC filter on the computer, a computational problem was noticed whose solution was not required in the 1-D simulations of Grossberg and Rudd (1989a, 1992). In particular, Figure 11 shows short-range spatial filtering of sustained cell outputs before gating the result with a transient on-cell or off-cell. The different spatial layouts of sustained cells in Figure 14 made it difficult to select a regular spatial arrangement of transient cells that could be used for all cases. This analysis suggested that each sustained cell is first gated by a transient on-cell and off-cell at its own location before each sustained-transient cell inputs to the several directionally-sensitive spatial filters to which it contributes. While these 2-D simulation problems were being confronted, Grossberg (1990, 1991, this
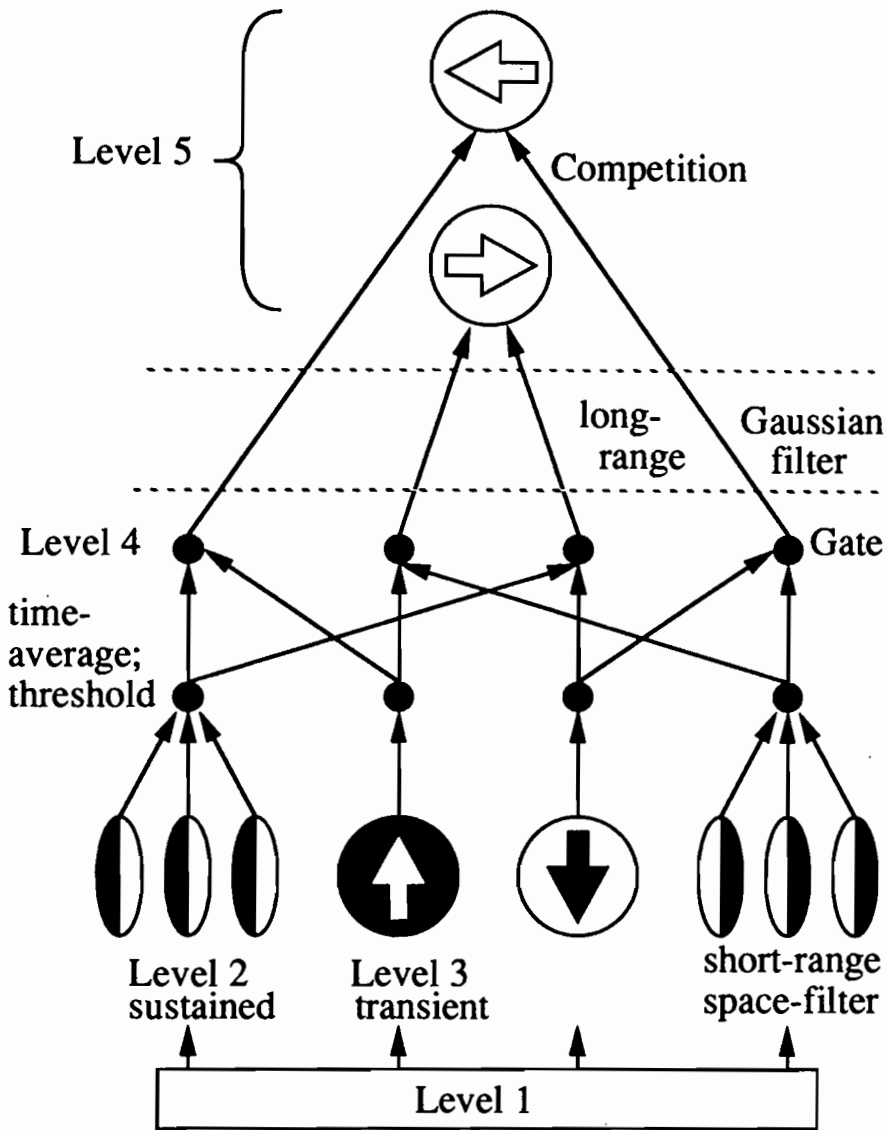
Figure 11: The Motion Oriented Contrast (MOC) Filter: Level 1 registers the input pattern. Level 2 consists of sustained response cells with oriented receptive fields that are sensitive to direction-of-contrast. Level 3 consists of transient response cells with unoriented receptive fields that are sensitive to direction-of-change in the total cell input. Level 4 cells combine sustained cell and transient cell signals to become sensitive to direction-of-motion and sensitive to direction-of-contrast. Level 5 cells combine Level 4 cells to become sensitive to direction-of-motion and insensitive to direction-of-contrast.
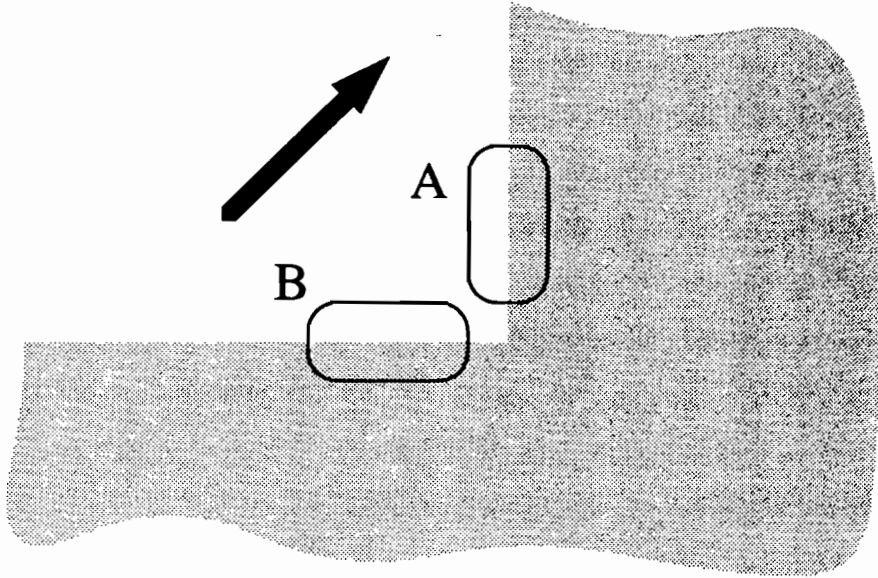
Figure 12: The lower right corner of a horizontally oriented rectangular region of homogeneous high luminance moves diagonally upward and to the right over a background of homogeneous low luminance. In region A a dark-to-light (luminance increasing over time) transition occurs at a vertical edge, while in region B a light-to-dark (luminance decreasing over time) transition occurs at a horizontal edge.

volume) observed that the FM Symmetry principle requires a similar spatial arrangement. We therefore modify the MOC Filter, as in Figure 15, by computing all sustained-transient combinations at each position before combining their outputs via directionally sensitive short-range spatial filters.

9. Endstopping: Generation of a Terminator or Corner Advantage in Motion Signals

Another 2-D MOC Filter refinement involves an *endstopping* operation. The need for this was illustrated in our discussion of the barberpole illusion in Section 1. There we noted that motion signals near terminators or corners tend to be better indicators of object motion than signals generated from a relatively straight interior of a contour. In order for a motion signal at a terminator or corner to be effective, however, it must somehow be translated into a relatively large signal strength, since the region of ambiguous interior motion signals is often larger than the region of unambiguous terminator or corner motion signals.

We suggest that one source of this enhancement involves endstopping the sustained cells and/or the transient cells of the MOC Filter. Many simple cells, identified with cells at
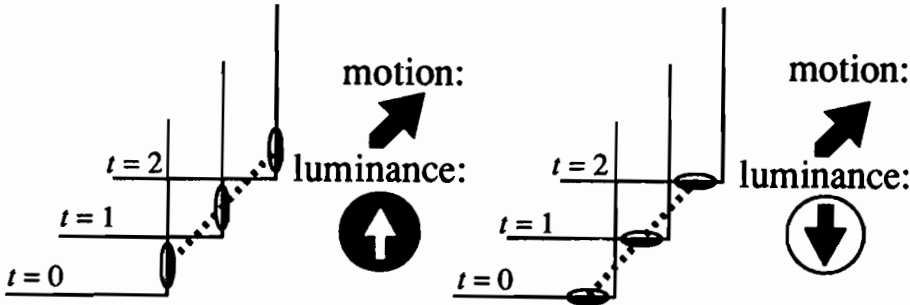
Figure 13: Over three successive time steps, the contours of the rectangle occupy the positions indicated, while luminance increases along the vertical edge and decreases along the horizontal edge. If certain of the sustained cell receptive fields sending inputs to Level 4 of the MOC Filter were arranged as indicated, a diagonal motion signal could be generated from both vertically and horizontally oriented cells, in conjunction with luminance gating signals of opposite signs.

Levels 2 and/or 4 of the MOC Filter, exhibit endstopping (Dreher, 1972). Endstopping is often informally described as consisting of inhibitory zones that occur along the major axis of orientationally tuned cells, beyond the contrast summing region, as indicated in Figure 16a. If this were all that was involved, then the end of a contrast edge that is oblique to a cell's preferred direction and partially overlaps the cell could escape the inhibitory zone and stimulate the cell more than a corresponding edge of the preferred direction (Figure 16b). This problem arises because the inhibition is anisotropic—that is, occurs only from the directions aligned with the cell's orientational axis.

    The anatomical substrate for such anisotropy would be more difficult to implement than a scheme of isotropic inhibition among orientationally tuned cells. For such an isotropic inhibitory scheme (Figure 17), the *observed* inhibitory zones for stimulation with edge stimuli would still appear only at the ends of the cell's receptive field, owing to the interaction between isotropic inhibition and oriented receptive fields.

    As illustrated in Figure 18a, strong endstopping can attenuate signals from all but the ends of a contour. Strong endstopping reduces the problem of determining motion direction to one of tracking an isolated region of activity in an upward diagonal direction, as in Figure 18b. Weak endstopping, as in Figure 18c, can partially attenuate interior signals, relative to signals at the ends. If endstopping is too weak, however, surviving signals indicating the "locally preferred" rightward horizontal direction can at least partially confound the computation of an upward diagonal object motion, as illustrated in Figure 18d. Marshall (1990) has also invoked end stopping in his explanation of the barberpole illusion, though in a manner different from that outlined here.

to long-range filter
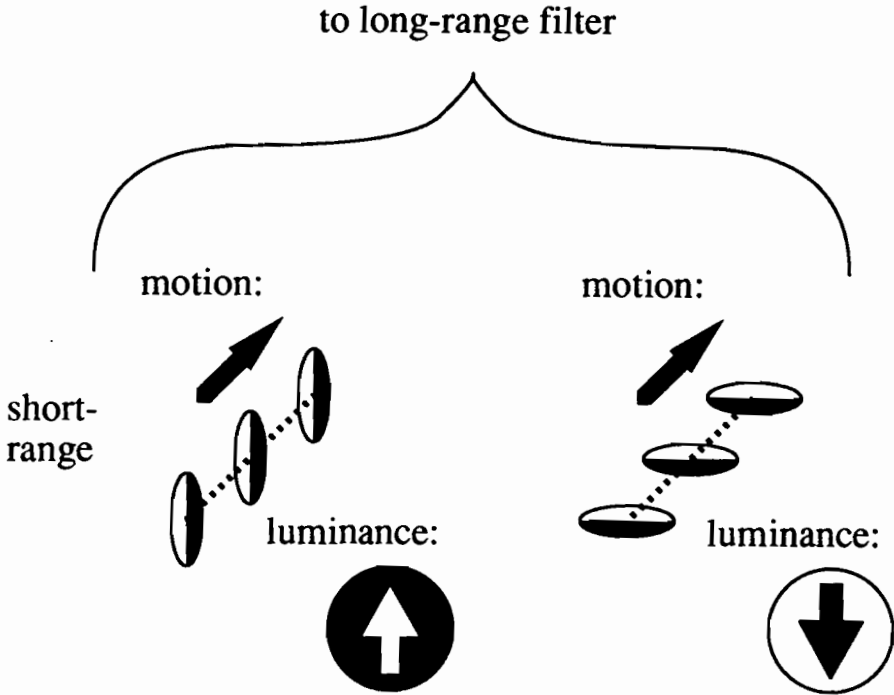
Figure 14: Signals arrive at the long-range filter (to Level 5 of the motion OC Filter) after several rectification and gating operations. Accordingly signals that were gated by both increases and decreases in luminance at (necessarily) different places can be combined into a coherent motion signal.

10. Directional Competition and Boundary Completion

The inward cooperative propagation by bipole cells of motion signals to locations between the strong end reactions can help to overcome this problem as it completes the motion signal along the entire contour (Figure 10). The cooperative feedback from the strong end reactions also leads to inhibition of other directional signals via short-range competition between directions at positions along the contour, as occurs during motion capture (see Section 2). Thus the type of CC Loop interactions among hypercomplex cells and bipole cells that help to select the globally preferred orientations in the Static BCS also help to select the globally preferred directions in the Motion BCS, with the caveat that "orientation" computations are replaced by "direction" computations.

11. 2-D MOC Filter Equations

We have found that several closely related computational realizations of the above heuristics can generate motion fields capable of distinguishing between contour orientation and con-
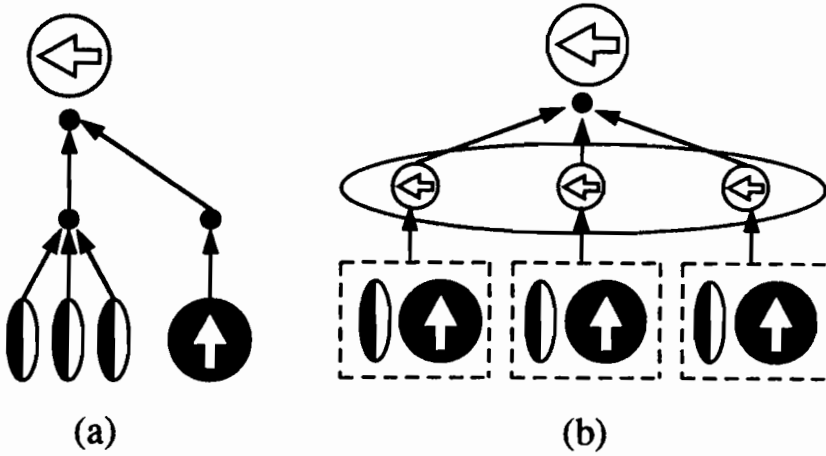
Figure 15: (a) The gating of sustained and transient cells within the MOC Filter of Grossberg and Rudd (1989a) was between several sustained cells (three shown) with aligned receptive field centers and a single transient cell. (b) The revised form of gating is one-to-one, between transient and sustained cells. Subsequently signals from spatially aligned gating cells (indicated by three small arrows) are pooled to form a single Level 4 signal.

tour direction-of-motion. We will here define a model that separates computations involving receptive fields with opposite directions-of-contrast until these are merged by the long-range Gaussian filter. This is the strategy followed by the Grossberg-Rudd model (Figure 11). Analogous properties have been simulated using a variant of this model in which receptive fields with opposite directions-of-contrast are merged at the short-range spatial filter stage (see Section 13). Other variations of the basic computational strategy also work, and might be used by different species *in vivo*. The description that follows is keyed to Figure 19.

Level 1: Stimulus Representation

Let $I_{pq}(t)$ denote the intensity of a time-varying image input at position (p, q) and time t.

Level 2: Oriented Sustained Receptive Fields

Let the output J_{ijk} of a receptive field centered at position (i, j) with orientation k be defined by

$$J_{ijk} = \sum_{pq} A_{ijpq}^{(k)} I_{pq} , \tag{1}$$

where $A_{ijpq}^{(k)}$ defines the value of a Gabor kernel at position (p, q) that is centered at position (i, j) with orientation k. The Gabor kernel is

$$A_{ijpq}^{(k)} = \alpha_A \ \exp\left[-\beta_A(\gamma_A\{B_{pqij}^{(k)}\}^2 + \{C_{pqij}^{(k)}\}^2)\right] \sin(\delta_A C_{pqij}^{(k)}), \tag{2}$$
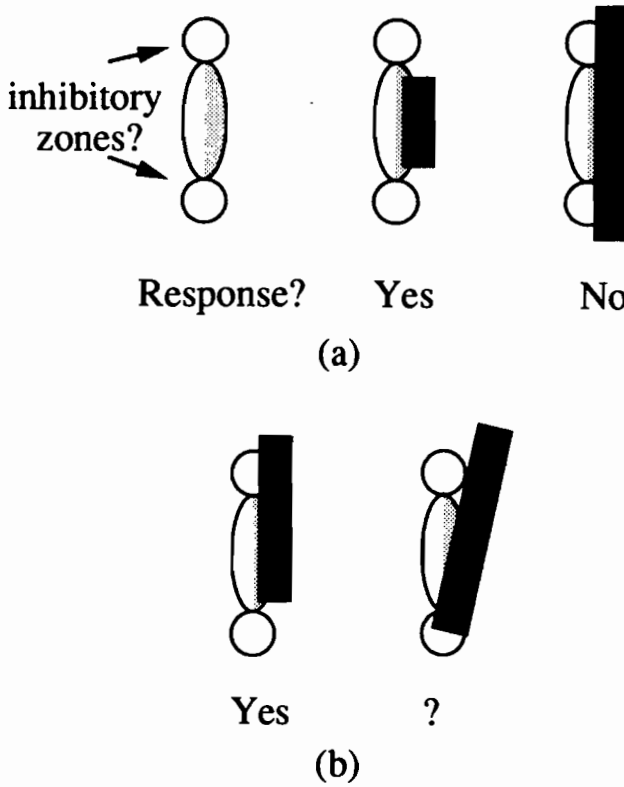
Figure 16: If the inhibitory end-zones of endstopped simple cells were laid out as caricatured in part (a), a cell would be unable to distinguish the termination of a line of its preferred orientation from the continuation of a line of an orientation slightly different from the cell's preferred orientation. In the resulting situation, diagrammed in (b), disinhibition of the (top) inhibitory zone occurs while the strength of response from the central region decreases.

where α_A is a constant that scales the Gabor amplitude, β_A scales the size of the kernel's Gaussian envelope, γ_A specifies the degree of elongation of the receptive field in the preferred orientation, and δ_A controls the frequency of the kernel's sinusoidal modulation. Terms

$$B_{ijpq}^{(k)} = (p-i)\cos(\frac{2\pi k}{K}) - (q-j)\sin(\frac{2\pi k}{K}) \tag{3}$$

and

$$C_{ijpq}^{(k)} = (p-i)\sin(\frac{2\pi k}{K}) + (q-j)\cos(\frac{2\pi k}{K}) \tag{4}$$
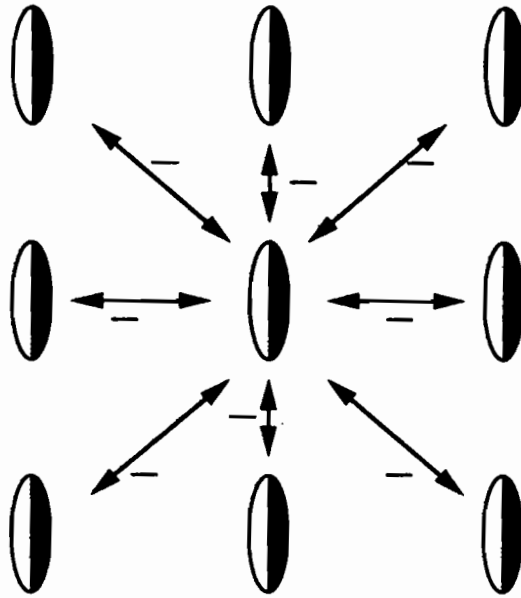
Figure 17: Spatially isotropic inhibition among like-oriented simple cells can generate functional enhancement of activity of oriented receptive fields near line ends or corners, often referred to as "endstopping."

describe the effect of shifting a receptive field centered at position $(0,0)$ to position (i,j), rotating it to orientation k, and evaluating it at position (p,q), given that K is the total number of orientations.

Level 3: Endstopped Sustained Cells

A competition of like-oriented Gabor receptive fields across neighboring positions and orientations leads to sustained cell activations x_{ijk} that are stronger at line ends and corners, as in equation

$$\frac{d}{dt}x_{ijk} = -\alpha_x x_{ijk} + (\beta_x - x_{ijk})J_{ijk} - (\gamma_x + x_{ijk}) \sum_{pq \in D_{ij}} J_{pqk}, \tag{5}$$

where D_{ij} is the set of all positions within some radius E of (i,j); that is,

$$D_{ij} = \left\{(p,q) : (p-i)^2 + (q-j)^2 \le E^2\right\}. \tag{6}$$

input   output

(a)

(b)

input   output

(c)

(d)
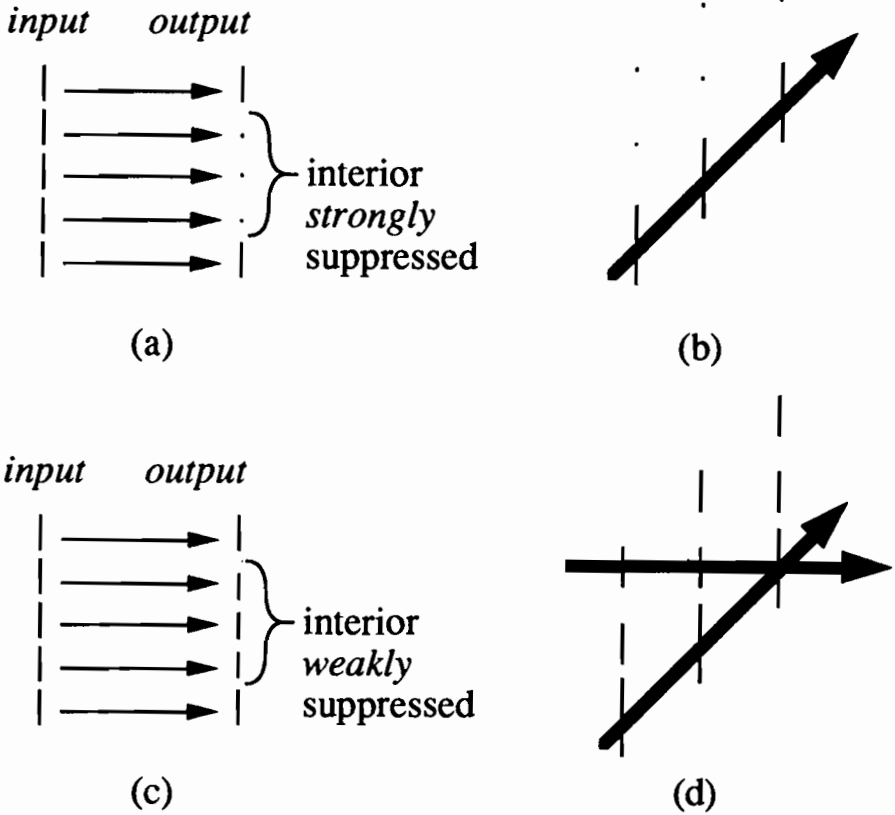
Figure 18: The enhancement of motion signals at line ends and corners can be strong or weak. (a) Strong inhibition can kill interior signals, making the problem of motion segmentation easy. (b) The surviving pools of activity at line ends can be directly tracked. (c) If endstopping is mild enough, however, locally preferred motion directions (perpendicular to edge contrast) survive, as shown in (d).

Level 4: Unoriented Transient Receptive Fields

The transient on-cell $y_{ij}^{(+)}$ responds to increments in the total input to a region F_{ij} surrounding (i, j), as in
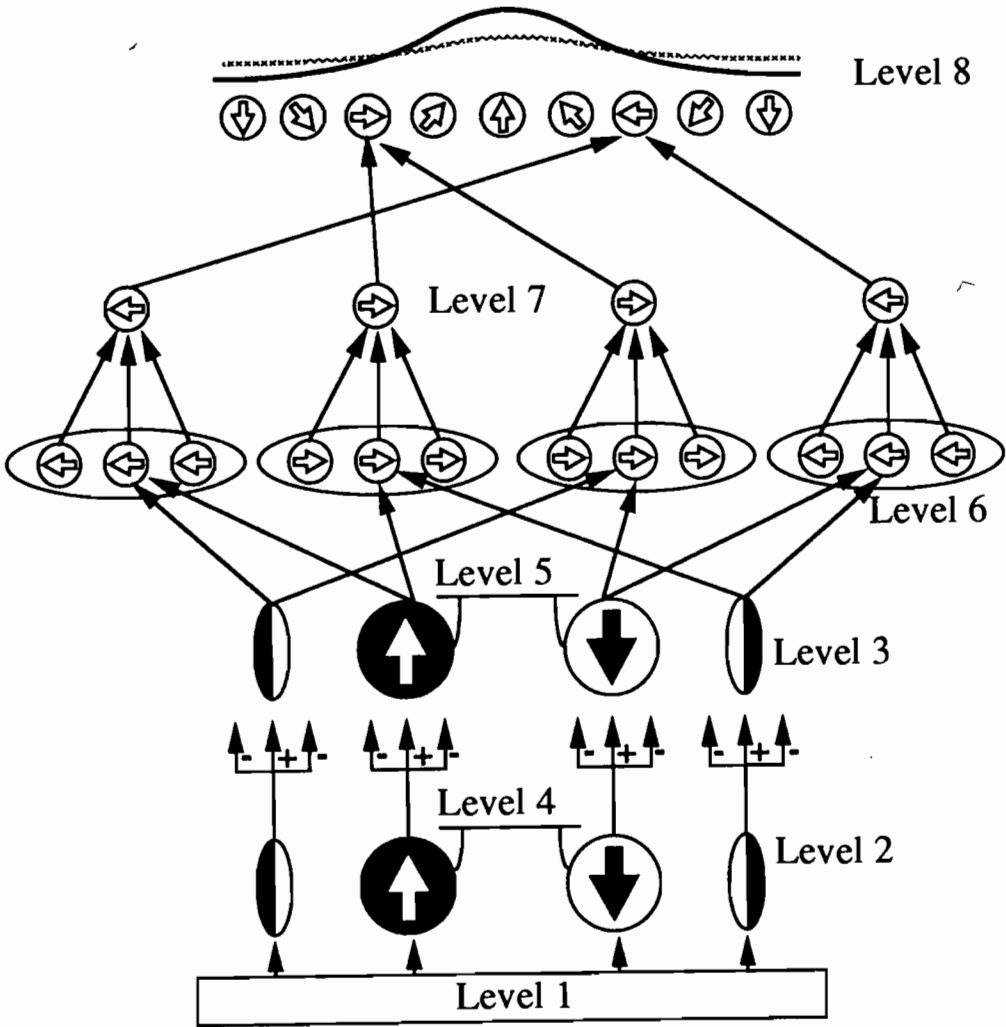
Figure 19: The 2-D MOC Filter embodies a number of variations and extensions of the architecture of the 1-D MOC Filter of Figure 11. See text for details.
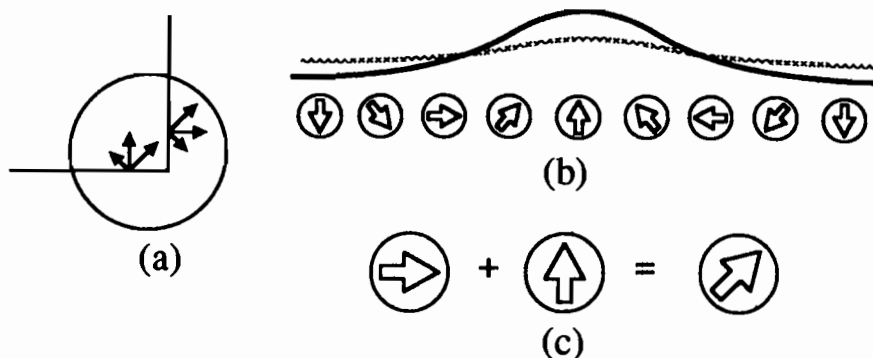
Figure 20: (a) At a corner the Gaussian filter combines signals of several directions. (The circle indicates the spatial domain of the Gaussian filter.) (b) The resolution of motion signals of many directions can be accomplished by a shunting "center-surround" competition with normalization among direction signals at a given location. Such a competition chooses the globally most consistent direction at a location. The solid line indicates the "on-center" and the dashed line the "off surround" of interaction weights across directions. (c) An input distribution with peaks at the rightward and upward directions is transformed into a single peaked distribution pointing upward and rightward by such a network.

$$y_{ij}^{(+)} = \Big[\frac{d}{dt} \sum_{pq \in F_{ij}} I_{pq} \Big]^+, \tag{7}$$

where F_{ij} is the set of all positions within some radius G of (i, j); that is,

$$F_{ij} = \{(p, q) : (p - i)^2 + (q - j)^2 \le G^2\} \tag{8}$$

for some radius G. Likewise, transient off-cell $y_{ij}^{(-)}$ responds to decrement in the total input to a region surrounding (i, j), as in

$$y_{ij}^{(-)} = \Big[-\frac{d}{dt} \sum_{pq \in F_{ij}} I_{pq} \Big]^+ \cdot \tag{9}$$

where region F_{ij} is defined above.

Level 5: Center-Surround Transient Cells

In this version of the model, lateral inhibition among transient cells, analogous to the endstopping operation among simple cells, is implemented. The center-surround transient cell activations $Y_{ij}^{(+)}$ and $Y_{ij}^{(-)}$ obey the same type of equation (5) as the endstopped sustained cells; namely,

$$\frac{d}{dt} Y_{ij}^{(+)} = -\alpha_y Y_{ij}^{(+)} + (\beta_y - Y_{ij}^{(+)}) y_{ij}^{(+)} - (\gamma_y + Y_{ij}^{(+)}) \sum_{pq \in H_{ij}} y_{pq}^{(+)} \tag{10}$$

and

$$\frac{d}{dt}Y_{ij}^{(-)} = -\alpha_y Y_{ij}^{(-)} + (\beta_y - Y_{ij}^{(-)})y_{ij}^{(-)} - (\gamma_y + Y_{ij}^{(-)}) \sum_{pq \in H_{ij}} y_{pq}^{(-)}, \tag{11}$$

where

$$H_{ij} = \left\{(p,q) : (p-i)^2 + (q-j)^2 \le L^2\right\}. \tag{12}$$

The transformation from Level 4 signals to Level 5 signals results in enhanced activity at line ends and corners.

Level 6: Sustained-Transient Simple Cells

As in Level 4 of the Grossberg-Rudd MOC Filter (Figure 11), multiplying outputs from sustained cells and transient cells starts to compute a local measure of motion direction. In particular, sustained cell activations that are sensitive to opposite directions-of-contrast give rise to activations that are sensitive to the same direction-of-motion by being multiplied with transient on-cells and off-cells, respectively. For example, the sustained-transient interaction

$$M_{ijm}^{(+)} = [x_{ijk}]^+ Y_{ij}^{(+)} \tag{13}$$

where

$$m = (k + \frac{K}{4}) \quad (mod \ K), \tag{14}$$

with K an integer multiple of 4, and the sustained-transient interaction

$$M_{ijm}^{(-)} = [x_{ij\hat{k}}]^+ Y_{ij}^{(-)} \tag{15}$$

where

$$\hat{k} = (k + \frac{K}{2}) \quad (mod \ K), \tag{16}$$

are both maximally sensitive to oriented contours of orientation k moving in direction m, even though the activations x_{ijk} and $x_{ij\hat{k}}$ sense opposite directions-of-contrast in an orientation that is perpendicular to m.

These quantities are time-averaged by the cells at which the sustained-transient interactions occur. Let $z_{ijm}^{(+)}$ and $z_{ijm}^{(-)}$ compute the activities of the sustained-transient cells which receive the inputs $M_{ijm}^{(+)}$ and $M_{ijm}^{(-)}$, respectively. Then

$$\frac{d}{dt}z_{ijm}^{(+)} = -\alpha_z z_{ijm}^{(+)} + M_{ijm}^{(+)} \tag{17}$$

and

$$\frac{d}{dt}z_{ijm}^{(-)} = -\alpha_z z_{ijm}^{(-)} + M_{ijm}^{(-)}. \tag{18}$$

For simplicity, the time averaging in (17) and (18) was computed in discrete time steps using equations

$$z_{ijm}^{(+)}(t) = \sum_{\tau=t-T}^{t} M_{ijm}^{(+)}(\tau)\zeta^{t-\tau}, \tag{19}$$
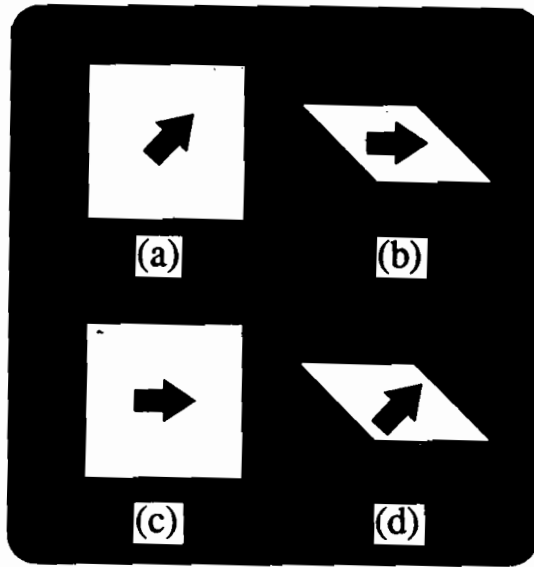
Figure 21: Simulations of the response of the 2-D MOC Filter to the motions of two simple figures are shown in subsequent figures. These figures are: (a) a square moving diagonally upward and to the right, (b) a parallelogram moving horizontally rightward, (c) a square moving horizontally rightward, and (d) a parallelogram moving diagonally up and to the right.

and

$$z_{ijm}^{(-)}(t) = \sum_{\tau=t-T}^{t} M_{ijm}^{(-)}(\tau)\zeta^{t-\tau}, \qquad (20)$$

where $0 < \zeta < 1$ and the number of time steps T was chosen large enough to provide a good approximation to (17) and (18), respectively. Comparison of the continuous and discrete time equations shows that $\zeta = \exp(-\alpha_z)$.

Level 7: Short-Range Spatial Filter: Pooling of Orientation Detectors into Local Direction Detectors

Each activation $z_{ijm}^{(+)}$ and $z_{ijm}^{(-)}$ is derived from an oriented receptive field whose orientation k is perpendicular to m. The next operation pools activations that are sensitive to the same direction-of-contrast using a short-range spatial filter. The spatial filter pools activations that lie along motion trajectories with different preferred directions-of-motion m. Activations $z_{ijn}^{(+)}$ or $z_{ijn}^{(-)}$ are accepted whose directions n are not too different from the trajectory direction m. This pooling operation exploits the relative advantage at line ends and corners achieved by endstopping to compute trajectory signals that begin to disambiguate a contour's direction-of-motion from its orientation.
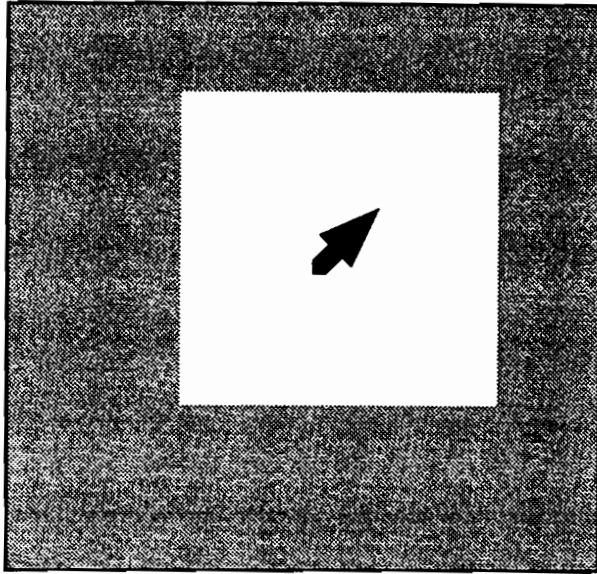
Figure 22: A representation of a frame from an input sequence presented to the 2-D MOC Filter. A light square moves diagonally up and to the right against a dark background. The resolution of the image used in the simulation was 128×128 pixels; the distance between nearest receptive field centers for network activities depicted in Figures 23–30 is four pixel units.

The short-range spatial kernel $N_{ijpq}^{(m,n)}$ favors a motion trajectory with direction-of-motion m that is centered at position (i, j). It separately pools activations $z_{pqn}^{(+)}$ or $z_{pqn}^{(-)}$ with a weight that depends upon how close n is to m and (p, q) is to (i, j), as in

$$u_{ijm}^{(+)} = \sum_{pqn} N_{ijpq}^{(m,n)} z_{pqn}^{(+)} \tag{21}$$

and

$$u_{ijm}^{(-)} = \sum_{pqn} N_{ijpq}^{(m,n)} z_{pqn}^{(-)}, \tag{22}$$

where

$$N_{ijpq}^{(m,n)} = P_{ijpq}^{(m)} \left[\cos(2\pi(m-n)K^{-1})\right]^{+} \tag{23}$$

and

$$P_{ijpq}^{(m)} = \alpha_p \exp\left[-\beta_p(\gamma_p\{Q_{ijpq}^{(m)}\}^2 + \{R_{ijpq}^{(m)}\}^2)\right] \cos(\delta_p R_{ijpq}^{(m)}). \tag{24}$$

In (24), just as in (2), α_p is a constant that scales the kernel amplitude, β_p determines the size of the kernel envelope, γ_p specifies the degree of kernel elongation in the preferred
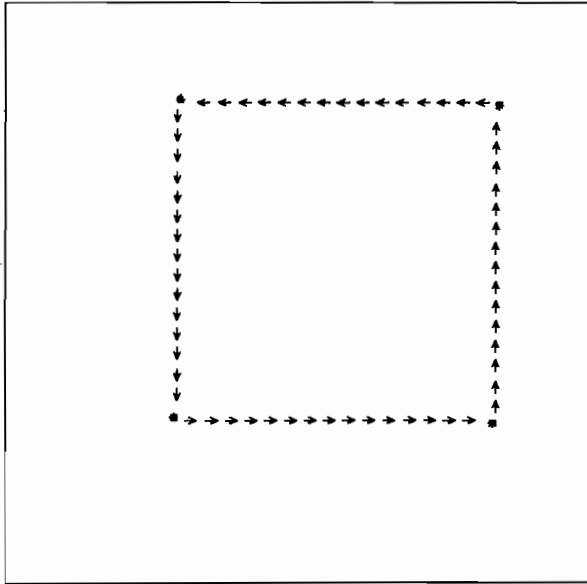
Figure 23: The output of the sustained cells of Level 2 in response to the moving square of Figure 22.
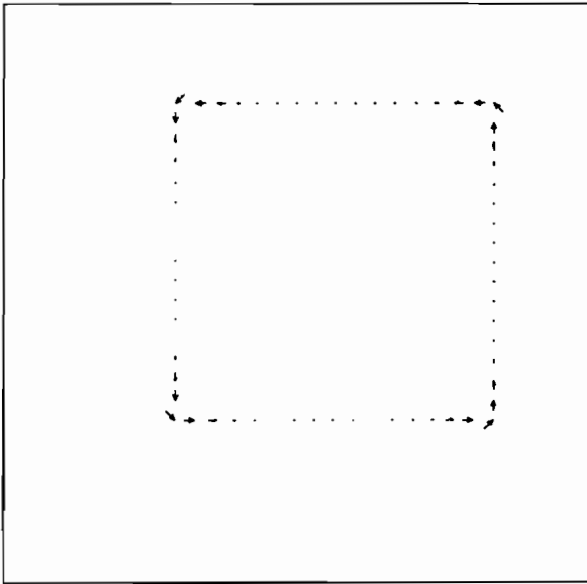
**Figure 24:** The output of the end-stopped sustained cells of Level 3 in response to the moving square of Figure 22.
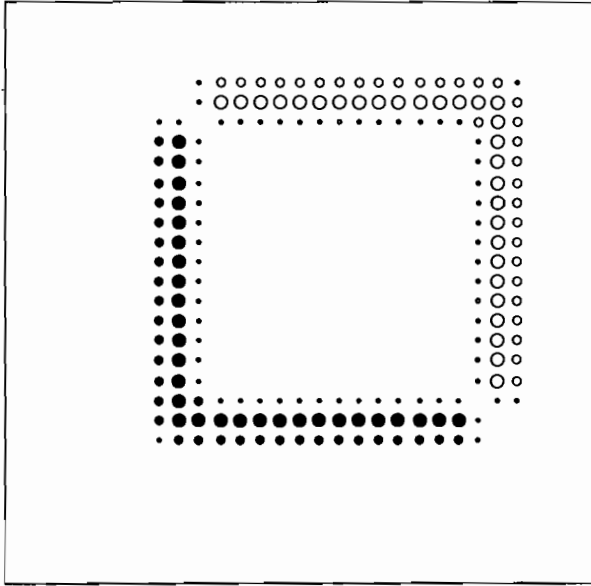
Figure 25: The output of the transient cells of Level 4 in response to the moving square of Figure 22.
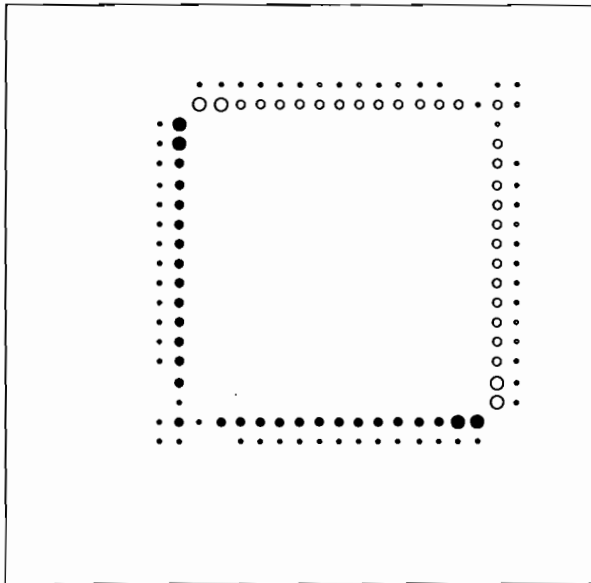
**Figure 26:** The output of the contrast-enhanced transient cells of Level 5 in response to the moving square of Figure 22.
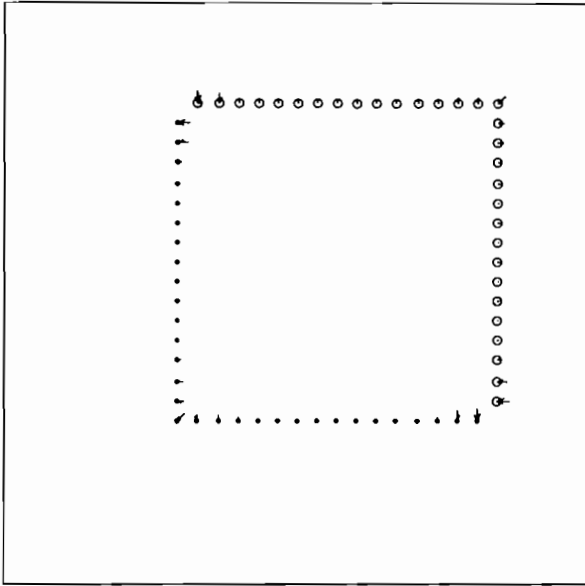
Figure 27: The output of the sustained-transient simple cells of Level 6 in response to the moving square of Figure 22.
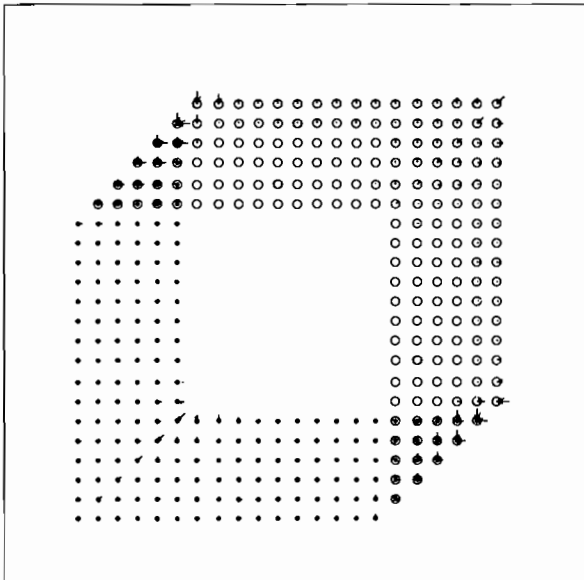
Figure 28: The pattern formed by the temporal smearing of the responses of sustained-transient simple cells of Level 6 to the moving square of Figure 22.
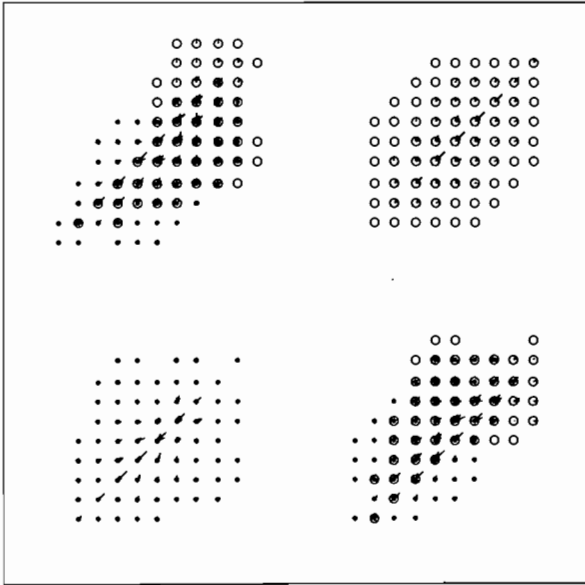
Figure 29: The output of the short-range spatial filter cells of Level 7 in response to the moving square of Figure 22.
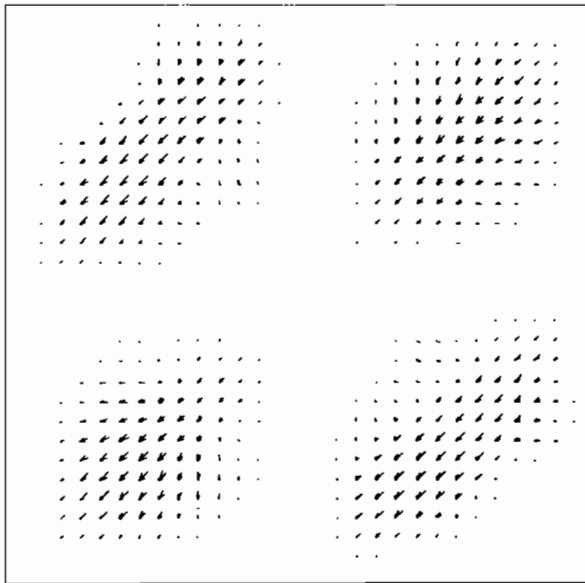
Figure 30: The output of the competitive cells of Level 8 in response to the moving square of Figure 22.

direction m, and δ_p specifies the frequency of the kernel's cosine modulation. The values

$$Q_{pqij}^{(m)} = (p-i)\cos(\frac{2\pi m}{K}) - (q-j)\sin(\frac{2\pi m}{K}) \tag{25}$$

and

$$R_{pqij}^{(m)} = (p-i)\sin(\frac{2\pi m}{K}) + (q-j)\cos(\frac{2\pi m}{K}) \tag{26}$$

describe the effect of shifting a receptive field centered at position $(0,0)$ to position (i,j), rotating it to point in direction m, and evaluating it at position (p,q).

The cell activations $u_{ijm}^{(+)}$ and $u_{ijm}^{(-)}$ are computed using algebraic equations (21) and (22) rather than the differential equations (17) and (18) used to compute $z_{ijm}^{(+)}$ and $z_{ijm}^{(-)}$, because $u_{ijm}^{(+)}$ and $u_{ijm}^{(-)}$ are assumed to respond much more quickly to their inputs than $z_{ijm}^{(+)}$ and $z_{ijm}^{(-)}$. In particular, the kernel $N_{ijpq}^{(m,n)}$ accumulates evidence for motion in direction m along a trajectory through position (i,j). The persistence of $z_{pqn}^{(+)}$ and $z_{pqn}^{(-)}$ activations as they temporally decay, together with the spatial anisotropy of the kernel, begin to overcome the uncertainties that arise from the aperture problem. Kernel anisotropy is hypothesized to arise, at least in part, in response to experiences with the trajectories of moving contours during an early phase of brain development. Such trajectories are, with high probability, approximately straight over sufficiently small regions.

The cell activations $u_{ijm}^{(+)}$ and $u_{ijm}^{(-)}$ both detect an estimate of direction-of-motion m at position (i,j), but they are sensitive to opposite directions-of-contrast. The long-range spatial filter combines signals that are sensitive to opposite directions-of-contrast, but the same direction-of-motion, to compute a more accurate estimate of motion direction, as indicated in Figure 17. The output signals $U_{ijm}^{(+)}$ and $U_{ijm}^{(-)}$ from Level 7 to this long-range filter are rectified versions of the Level 7 activations, as in

$$U_{ijm}^{(+)} = [u_{ijm}^{(+)} - \eta]^+ \tag{27}$$

and

$$U_{ijm}^{(-)} = [u_{ijm}^{(-)} - \eta]^+. \tag{28}$$

Level 8: Long-Range Spatial Filter and Directional Competition

The trajectory responses $U_{ijm}^{(+)}$ and $U_{ijm}^{(-)}$ are next combined across space and direction-of-contrast to generate a response ν_{ijm} that is sensitive to the consensus within a region surrounding position (i,j) of how much evidence there exists for motion in direction m. Thus we let

$$\nu_{ijm} = \sum_{pq \in W_{ij}} (U_{pqm}^{(+)} + U_{pqm}^{(-)}) \exp\{-\alpha_\nu[(p-i)^2 + (q-j)^2]\}, \tag{29}$$

where

$$W_{ij} = \{(p,q) : (p-i)^2 + (q-j)^2 \le X^2\}. \tag{30}$$
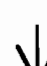
| Symbol	Figures	Level	Cell Type
↓	23, 32	2	oriented sustained
↓	24, 33	3	end-stopped oriented sustained
●	25, 34	4	unoriented transient (luminance decreasing)
○	25, 34	4	unoriented transient (luminance increasing)
●	26, 35	5	center-surround transient (luminance decreasing)
○	26, 35	5	center-surround transient (luminance increasing)
↓●	27, 36	6	sustained-transient simple (luminance decreasing)
↓○	27, 36	6	sustained-transient simple (luminance increasing)
↓●	28, 37	6	time-average of sustained-transient simple (luminance decreasing)
↓○	28, 37	6	time-average of sustained-transient simple (luminance increasing)
↓●	29, 38	7	short-range spatial filter (luminance decreasing)
↓○	29, 38	7	short-range spatial filter (luminance increasing)
↓	30, 39, 41, 43	8	motion hypercomplex

Table 1.
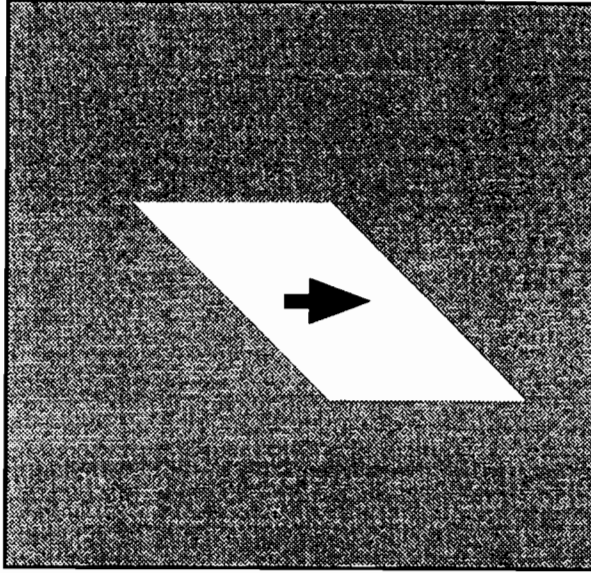
Figure 31: A representation of a frame from an input sequence presented to the 2-D MOC Filter. A light parallelogram moves rightward against a dark background. The resolution of the image used in the simulation was 128×128 pixels; the distance between nearest receptive field centers for network activities depicted in Figures 32–39 is four pixel units.

The output of the long-range filter undergoes a final competition to choose a consensual direction among all signals which have been grouped at a spatial location (Figure 20). This competition is in the form of a "center-surround" organization in "direction space," as given by

$$\frac{d}{dt} w_{ijm} = -\alpha_w w_{ijm} + (\beta_w - w_{ijm}) \sum_n \nu_{ijn} \gamma_{nm} - (\delta_w + w_{ijm}) \sum_n \nu_{ijn} \epsilon_{nm} \qquad (31)$$

where

$$\gamma_{nm} = \gamma \exp[-\mu_w (m - n)^2] \qquad (32)$$

and

$$\epsilon_{nm} = \epsilon \exp[-\nu_w (m - n)^2]. \qquad (33)$$

The competition stage at Level 8 is not necessary to generate consistent direction signals for simple, noise-free inputs. Snowden (1989, 1990) has reported psychophysical and physiological evidence for such shunting inhibition among directional signals, for situations in which conflicting signals must be resolved. Williams and Phillips (1987) and Watson and Ahumada (1985) have proposed a similar direction-averaging mechanism.
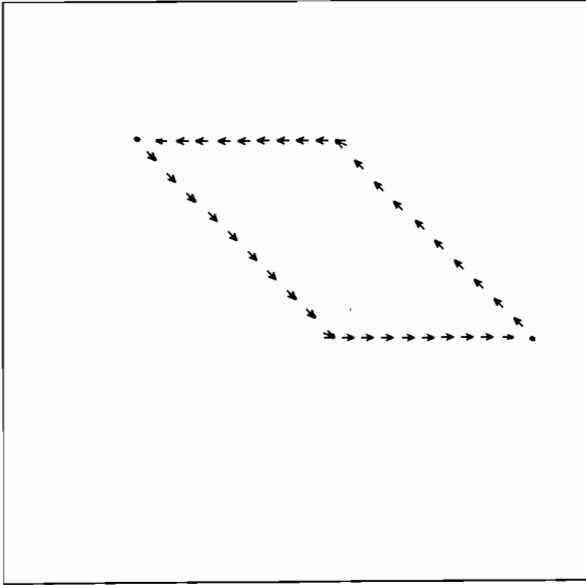
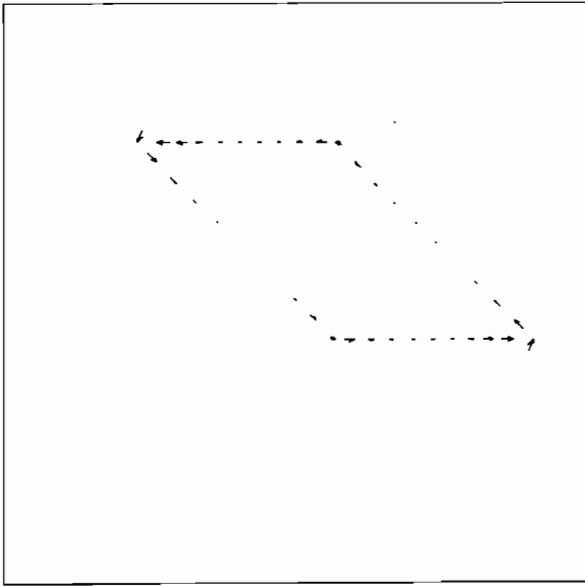**Figure 32:** The output of the sustained cells of Level 2 in response to the moving parallelogram of Figure 31.

Figure 33: The output of the end-stopped sustained cells of Level 4 in response to the moving parallelogram of Figure 31.
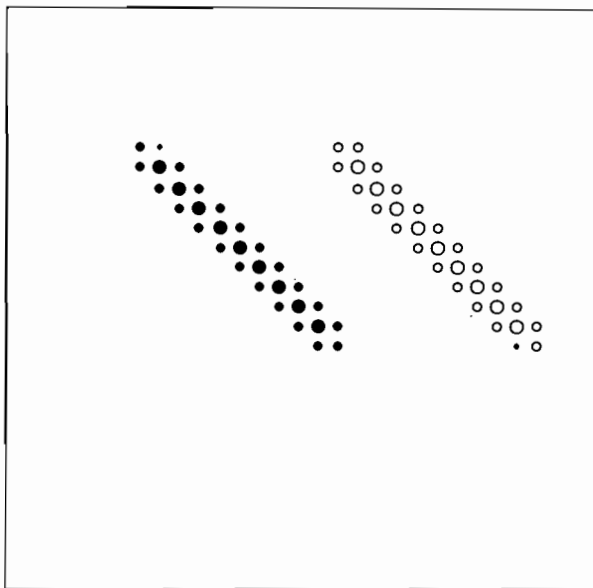
Figure 34: The output of the transient cells of Level 4 in response to the moving parallelogram of Figure 31.
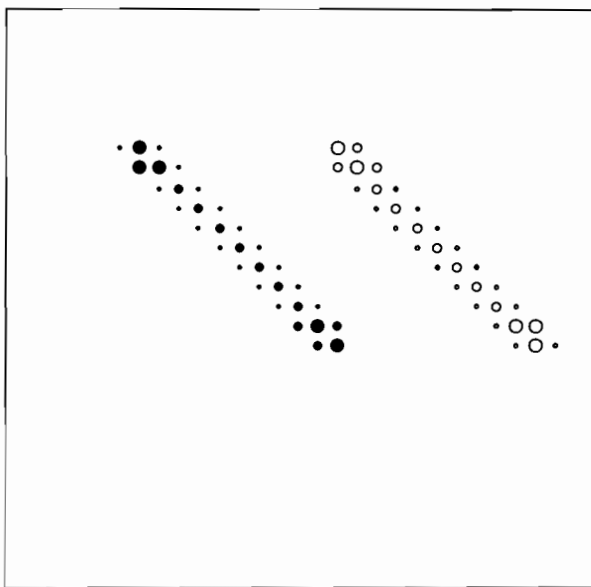
Figure 35: The output of the contrast-enhanced transient cells of Level 5 in response to the moving parallelogram of Figure 31.

Figure 36: The output of the sustained-transient simple cells of Level 6 in response to the moving parallelogram of Figure 31.

Figure 37: The pattern formed by the temporal smearing of the responses of sustained-transient simple cells of Level 6 to the moving parallelogram of Figure 31.

Figure 38: The output of the short-range spatial filter cells of Level 7 in response to the moving parallelogram of Figure 31.

Figure 39: The output of the competitive cells of Level 8 in response to the moving parallelogram of Figure 31.
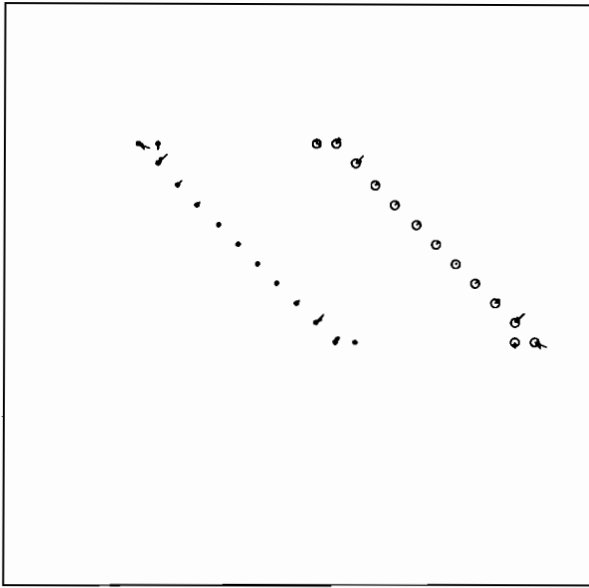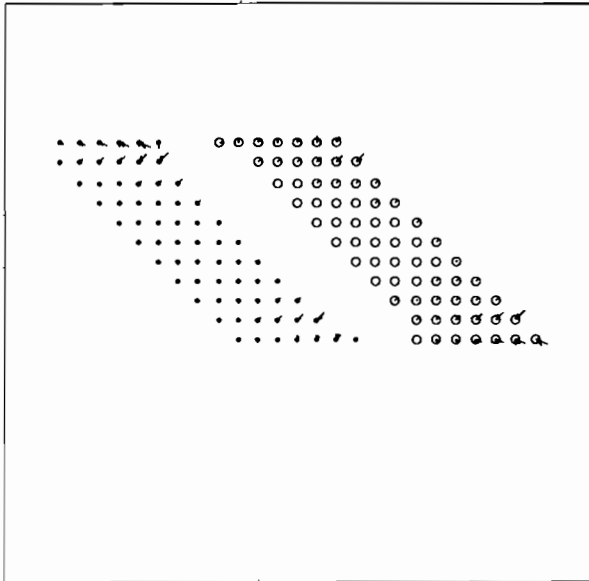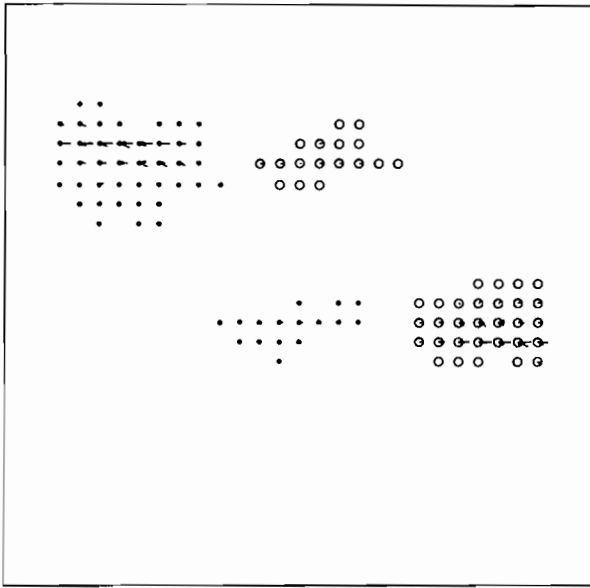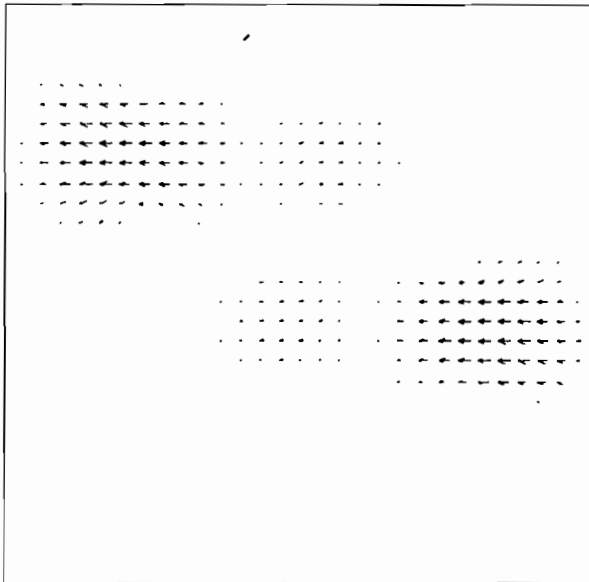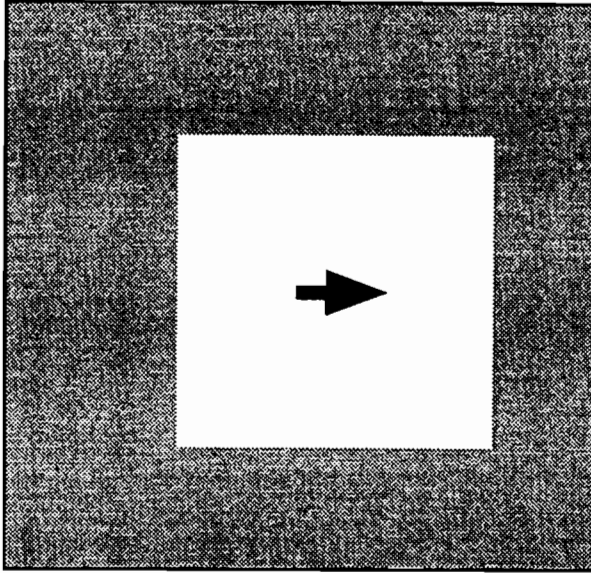
Figure 40: A representation of a frame from an input sequence presented to the 2-D MOC Filter. A light square moves horizontally to the right against a dark background. The resolution of the image used in the simulation is 128 × 128 pixels; the distance between nearest receptive field centers for network activities depicted in Figure 41 is four pixel units.

12. Computer Simulations: Distinguishing Motion Direction from Boundary Orientation

Computer simulations were carried out on simple moving forms to illustrate how the MOC Filter can compute an accurate measure of motion direction even if the bounding contours of the form have orientations that are not perpendicular to the direction of motion. Four illustrative moving forms are analysed below: a rectangle moving diagonally upward; a rectangle moving to the right; a rhombus moving diagonally upward; and a parallelogram moving to the right (Figure 21). For the square moving diagonally, the resultant activation pattern at each stage of the MOC Filter is shown in order to aid the reader's intuition. The graphics conventions used are shown in Table 1.

Consider the case of a light square moving diagonally up and to the right on a dark background, as depicted in Figure 22. Figure 23 displays the response of the oriented sustained detectors of Level 2; the parameters controlling the scale of the detectors are such that only a single row or column is activated around the perimeter of the square, although several orientations are active at each position. Figure 24 displays the response of the end-stopped, oriented sustained detectors of Level 3. Note the attenuated response along the interiors of the segments bounding the square, and the enhanced response at corners. Figure 25 displays the response of increasing and decreasing transient detectors of Level 4. Note that the leading and trailing corners (upper right and lower left, respectively) have strong activity,
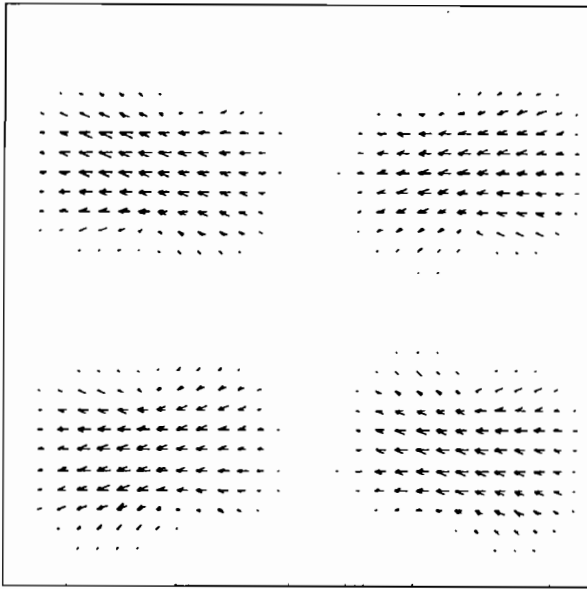
Figure 41: The output of the competitive cells of Level 8 in response to the moving square of Figure 40.

because the axis they define is in the direction of motion, while the other two corners have attenuated activity. Figure 26 displays the result of contrast enhancing competition of Level 5 transient detectors. Note that this competition occurs independently in the "increasing" and "decreasing" channels, permitting the greatest enhancement of activity at the corners where activity was weakest in Figure 25.

   Figures 31–39 display a sequence of transformations corresponding to those of Figures 23–30, but this time for the case of a rhombus moving horizontally to the right, as depicted in Figure 31. The transformation from the output of oriented sustained cells of Level 2, shown in Figure 32, to the output of end-stopped cells of Level 3, shown in Figure 33, changes the relative distribution of active orientations at corners. Likewise, the transformation from Level 4 transient cells to Level 5 contrast-enhanced transient cells, shown in Figures 34 and 35 respectively, helps to create a stronger pool of activity at the ends of the diagonal lines, as was discussed with reference to the barberpole illusion in Section 2. The output of transient-sustained simple cells of Level 6, shown in Figure 36, contains an assortment of active local direction signals. The spatial trail formed by the smearing of those signals in time, shown in Figure 37, enables the short-range spatial filters of Level 7, shown in Figure 38, to more accurately register the prevailing direction of motion. The output of Level 8, shown in Figure 39, further smooths the signals over space, while sharpening their directional distribution. Note that the resulting pattern of activity is stronger at the 45° corners than at the 135° corners, and that the directional pattern at the latter is not symmetric about the horizontal. It may be that such effects underlie some of the anomalous motion percepts reported for
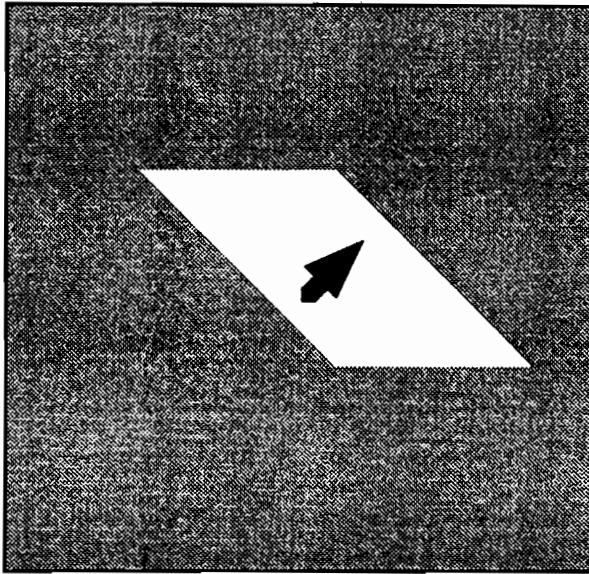
Figure 42: A representation of a frame from an input sequence presented to the 2-D MOC Filter. A light parallelogram moves diagonally up and to the right against a dark background. The resolution of the image used in the simulation was 128 × 128 pixels; the distance between nearest receptive field centers for network activities depicted in Figure 43 is four pixel units.

motions of curves such as those employed by Nakayama and Silverman (1988). Changing parameters in the simulation to include longer spatial filters at Level 7 would in any case reduce this effect and generate a more nearly horizontal pattern of responses.

For comparison, we have included the response at Level 8 to the cases where a horizontal square moves rightward (Figures 40 and 41) and where a parallelogram moves diagonally (Figures 42 and 43).

13. A Related MOC Filter

Similar computational properties are found if the mask responses in (1) are thresholded, as in

$$J_{ijk} = \left[\sum_{pq} A^{(k)}_{ijpq} I_{pq} - \epsilon_A \right]^+, \tag{31}$$

and the terms $M^{(+)}_{ijm}$ in (13) and $M^{(-)}_{ijm}$ in (15) are combined into a single time-averaged sustained-transient cell type z_{ijm}, instead of the separate streams (19) and (20). Then

$$z_{ijm}(t) = \sum_{\tau=t-T}^{t} (M^{(+)}_{ijm}(\tau) + M^{(-)}_{ijm}(\tau)) \zeta^{t-\tau} \tag{32}$$
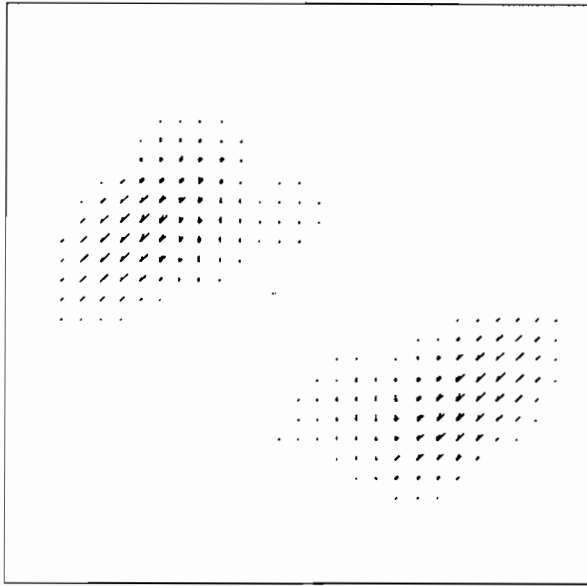
Figure 43: The output of the competitive cells of Level 8 in response to the moving parallelogram of Figure 42.

and

$$u_{ijm} = \sum_{pqn} \overline{N}_{ijpq}^{(m,n)} z_{pqn}, \tag{33}$$

where

$$\overline{N}_{ijpq}^{(m,n)} = P_{ijpq}^{(m)}\left\{[\cos(2\pi(m-n)K^{-1})]^+\right\}^p, \tag{34}$$

function P_{ijpq} is defined in (23), and parameter p in (34) enables the smoothing across directions n to be made more or less broad within a 180-degree span. Using this approach, the threshold η in (27) and (28) is not needed, because the masks (31) are already thresholded, and the functions $M_{ijm}^{(+)}$ and $M_{ijm}^{(-)}$ combine to generate a more central directional tendency at an early processing stage. Then

$$\nu_{ijm} = \sum_{pq\epsilon W} u_{pqm} \, \exp\left\{-\alpha_\nu[(p-i)^2 + (q-j)^2]\right\} \tag{35}$$

suffices instead of (29).

14. Perception of Moving-Form-in-Depth: The V1 → V2 → MT Pathway

The Motion BCS circuitry suggests the types of processing stages, and their ordering, that are needed to effectively process moving images. As such, the circuit suggests experimental tests of the cell types and interactions in the $V1 \rightarrow MT$ cortical processing stream.

Motion BCS   *Static BCS*

CC Loop   CC Loop

↑ ↓   ↑ ↓

MOC Filter   SOC Filter
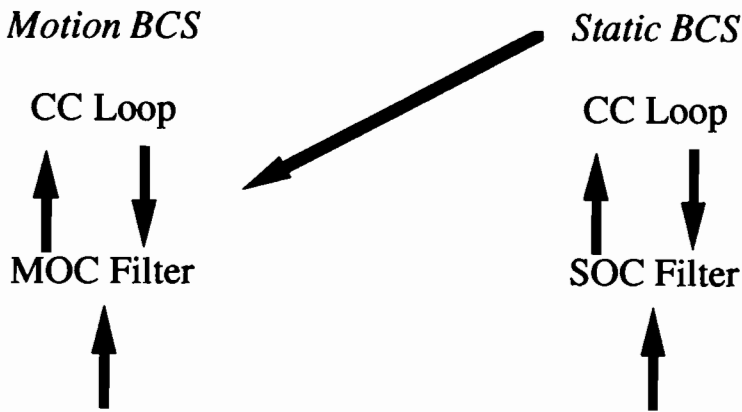
↑   ↑

Figure 44: Model analog of $V1 \rightarrow V2 \rightarrow MT$ pathway: Stereo-sensitive emergent segmentations from the Static CC Loop help to select the depthfully correct combinations of motion signals in the MOC Filter.

The theory also helps to understand why an indirect, $V1 \rightarrow V2 \rightarrow MT$, cortical pathway from V1 to MT exists in addition to the direct $V1 \rightarrow MT$ pathway (DeYoe and van Essen, 1988) (Figure 44). As noted in Section 7, outputs from the MOC Filter sacrifice a measure of orientational specificity in order to effectively process direction-of-motion. However, precisely oriented binocular matches are important in the selection of cortical cells that are tuned to the correct binocular disparities (von der Heydt, Hänny, and Dürsteler, 1981). The Static BCS can carry out such precise oriented matches; the Motion BCS cannot. This fact suggests that a pathway from the Static BCS to the Motion BCS exists in order to help the Motion BCS to generate its motion segmentations at correctly calibrated depths.

Such a pathway needs to arise after the level of BCS processing at which cells capable of binocular fusion are chosen and binocularly rivalrous cells are suppressed. This occurs within the hypercomplex cells and bipole cells of the Static BCS (Grossberg, 1987b; Grossberg and Marshall, 1989), hence within the model analog of prestriate cortical area V2 (Figure 44). Thus the existence of a pathway from V2 and/or V4 to MT is consistent with the different functional roles of the Static BCS and the Motion BCS.

According to this reasoning, the $V2 \rightarrow MT$ pathway should occur at a processing stage prior to the one at which several orientations are pooled into a single direction-of-motion within each spatial scale. Thus, the pathway ends in the MOC Filter at a stage no later than Level 4 in Figure 11, or correspondingly, Level 7 in Figure 19. Such a pathway would join like orientations within like spatial scales between the Static BCS and the Motion BCS. It could thereby enhance the activation within the Motion BCS of those spatial scales and orientations that are binocularly fused within the Static BCS.

REFERENCES

Adelson, E.H. and Movshon, J.A. (1982). Phenomenal coherence of moving visual patterns. *Nature*, **300**, 523–525.

Albright, T.D., Desimone, R., and Gross, C.G. (1984). Columnar organization of directionally sensitive cells in visual area MT of the macaque. *Journal of Neurophysiology*, **51**, 16–31.

Anderson, S.J. and Burr, D.C. (1987). Receptive field size of human motion detection units. *Vision Research*, **27**, 621–635.

Anstis, S.M. and Mather, G. (1985). Effects of luminance and contrast on direction of ambiguous apparent motion. *Perception*, **14**, 167–179.

Anstis, S.M. and Ramachandran, V.S. (1987). Visual inertia in apparent motion. *Vision Research*, **27**, 755–764.

Braddick, O.J. (1974). A short range process in apparent motion. *Vision Research*, **14**, 519–527.

Burr, D.C., Ross, J., and Morrone, M.C. (1986). Smooth and sampled motion. *Vision Research*, **26**, 643–652.

Carpenter, G.A., Grossberg, S., and Mehanian, C. (1989). Invariant recognition of cluttered scenes by a self-organizing ART architecture: CORT-X boundary segmentation. *Neural Networks*, **2**, 169–181.

Cohen, M.A. and Grossberg, S. (1984). Neural dynamics of brightness perception: Features, boundaries, diffusion, and resonance. *Perception and Psychophysics*, **36**, 428–456.

Derrington, A. and Suero, M. (1991). Motion of complex patterns is computed from the perceived motions of their components. *Vision Research*, **31**(1), 139–150.

DeValois, R.L., Albrecht, D.G., and Thorell, L.G. (1982). Spatial frequency selectivity of cells in macaque visual cortex. *Vision Research*, **22**, 545–559.

DeYoe, E.A. and van Essen, D.C. (1988). Concurrent processing streams in monkey visual cortex. *Trends in Neuroscience*, **11**, 219–226.

Dreher, B. (1972). Hypercomplex cells in the cat's striate cortex. *Investigative Ophthalmology*, **11**, 355–356.

Eckhorn, R., Bauer, R., Jordan, W., Brosch, M., Kruse, W., Munk, M., and Reitboeck, H.J. (1988). Coherent oscillations: A mechanism of feature linking in the visual cortex? *Biological Cybernetics*, **60**, 121–130.

Eskew, R.T., Jr., Stromeyer, C.F., III, Picotte, C.J., and Kronauer, R.E. (1991). Detection uncertainty and the facilitation of chromatic detection by luminance contours. *Journal of the Optical Society of America A*, **8**, 394–403.

Foster, K.H., Gaska, J.P., Nagler, M., and Pollen, D.A. (1985). Spatial and temporal frequency selectivity of neurons in visual cortical areas V1 and V2 of the macaque monkey. *Journal of Physiology*, **365**, 331–363.

Gray, C.M., Konig, P., Engel, A.K., and Singer, W. (1989). Oscillatory responses in cat visual cortex exhibit inter-columnar synchronization which reflects global stimulus properties. *Nature*, **338**, 334–337.

Grossberg, S. (1973). Contour enhancement, short-term memory, and constancies in reverberating neural networks. *Studies in Applied Mathematics*, **52**, 217–257.

Grossberg, S. (1982). **Studies of mind and brain: Neural principles of learning, perception, development, cognition, and motor control**. Boston: Reidel Press.

Grossberg, S. (1987a). Cortical dynamics of three-dimensional form, color, and brightness perception, I: Monocular theory. *Perception and Psychophysics*, **41**, 87–116.

Grossberg, S. (1987b). Cortical dynamics of three-dimensional form, color, and brightness perception, II: Binocular theory. *Perception and Psychophysics*, **41**, 117–158.

Grossberg, S. (Ed.) (1987c). **The adaptive brain, II: Vision, speech, language, and motor control**. Amsterdam: Elsevier/North-Holland.

Grossberg, S. (1990). Neural facades: Visual representations of static and moving form-and-color-and-depth. *Mind and Language*, **5**, 411–456.

Grossberg, S. (1991). Why do parallel cortical systems exist for the perception of static form and moving form? *Perception and Psychophysics*, **49**, 117–141.

Grossberg, S. and Marshall, J. (1989). Stereo boundary fusion by cortical complex cells: A system of maps, filters, and feedback networks for multiplexing distributed data. *Neural Networks*, **2**, 29–51.

Grossberg, S. and Mingolla, E. (1985a). Neural dynamics of form perception: Boundary completion, illusory figures, and neon color spreading. *Psychological Review*, **92**, 173–211.

Grossberg, S. and Mingolla, E. (1985b). Neural dynamics of perceptual grouping: Textures, boundaries, and emergent segmentations. *Perception and Psychophysics*, **38**, 141–171.

Grossberg, S. and Mingolla, E. (1987). Neural dynamics of surface perception: Boundary webs, illuminants, and shape-from-shading. ·*Computer Vision, Graphics, and Image, Processing*, **37**, 116–165.

Grossberg, S., Mingolla, E., and Todorović, D. (1989). A neural network architecture for preattentive vision. *IEEE Transactions on Biomedical Engineering*, **36**, 65–84.

Grossberg, S. and Rudd, M.E. (1989a). A neural architecture for visual motion perception: Group and element apparent motion. *Neural Networks*, **2**, 421–450.

Grossberg, S. and Rudd, M.E. (1989b). Neural dynamics of visual motion perception: Group and element apparent motion. *Investigative Ophthalmology Supplement*, **30**, 73.

Grossberg, S. and Rudd, M.E. (1992). Cortical dynamics of visual motion perception: Short-range and long-range motion. *Psychological Review*, in press.

Grossberg, S. and Somers, D. (1991). Synchronized oscillations during cooperative feature linking in a cortical model of visual perception. *Neural Networks*, **4**, 453–466.

Grossberg, S. and Todorović, D. (1988). Neural dynamics of 1-D and 2-D brightness perception: A unified model of classical and recent phenomena. *Perception and Psychophysics*, **43**, 241–277.

Heggelund, P. (1981). Receptive field organization of simple cells in cat striate cortex. *Experimental Brain Research*, **42**, 89–107.

Hubel, D.H. and Wiesel, T.N. (1962). Receptive fields, binocular interaction and functional architecture in the cat's visual cortex. *Journal of Physiology*, **160**, 106–154.

Hubel, D.H. and Wiesel, T.N. (1968). Receptive fields and functional architecture of monkey striate cortex. *Journal of Physiology*, **195**, 215–243.

Hubel, D.H. and Wiesel, T.N. (1977). Functional architecture of macaque monkey visual cortex. *Proceedings of the Royal Society of London B*, **198**, 1–59.

Humphreys, G.W., Quinlan, P.T., and Riddoch, M.J. (1989). Grouping processes in visual search: Effects with single- and combined-feature targets. *Journal of Experimental Psychology: General*, **118**, 258–279.

Kellman, P.J. and Shipley, T.F. (1991). A theory of visual interpolation in object perception. *Cognitive Psychology*, **23**, 141–221.

Kennedy, J.M. (1979). Subjective contours, contrast, and assimilation. In C. F. Nodine and D. F. Fisher (Eds.) **Perception and pictorial representation**. Ney York: Praeger.

Lappin, J.S. and Bell, H.H. (1976). The detection of coherence in moving random-dot patterns. *Vision Research*, **16**, 161–168.

Livingstone, M.S. and Hubel, D.H. (1987). Psychophysical evidence for separate channels for the perception of form, color, movement, and depth. *Journal of Neuroscience*, **7**, 3416–3468.

Marr, D. and Ullman, S. (1981). Directional selectivity and its use in early visual processing. *Proceedings of the Royal Society of London B*, **211**, 151–180.

Marshall, J.A. (1990). Self-organizing neural networks for perception of visual motion. *Neural Networks*, **3**, 45–74.

Maunsell, J.H.R. and van Essen, D.C. (1983). Response properties of single units in middle temporal visual area of the macaque. *Journal of Neurophysiology*, **49**, 1127–1147.

Meyer, G.E. and Dougherty, T. (1987). Effects of flicker-induced depth on chromatic subjective contours. *Journal of Experimental Psychology: Human Perception and Performance*, **13**(3), 353–360.

Mikaelian, H.H., Linton, M.J., and Phillips, M. (1990). Orientation-specific luminance after-effects. *Perception and Psychophysics*, **47**(6), 575–582.

Mingolla, E., Todd, J.T., and Norman, F. (1992). The perception of globally coherent motion. *Vision Research*, in press.

Movshon, J.A., Adelson, E.H., Gizzi, M.S., and Newsome, W.T. (1985). The analysis of moving visual patterns. In C. Chagas, R. Gattas, and C. Gross (Eds.) **Pattern recognition mechanisms**. New York: Springer-Verlag.

Nakayama, K. and Silverman, G.H. (1984). Temporal and spatial characteristics of the upper displacement limit for motion in random dots. *Vision Research*, **24**, 293–299.

Nakayama, K. and Silverman, G.H. (1985). Detection and discrimination of sinusoidal grating displacements. *Journal of the Optical Society of America*, **2**, 267–273.

Nakayama, K. and Silverman, G.H. (1988). The aperture problem, II: Spatial integration of velocity information along contours. *Vision Research*, **28**(6), 747–753.

Newsome, W.T., Gizzi, M.S., and Movshon, J.A. (1983). Spatial and temporal properties of neurons in macaque MT. *Investigative Ophthalmology and Visual Sciences*, **24**, 106.

Paradiso, M. and Nakayama, K. (1991). Brightness perception and filling-in. *Vision Research*, **31**(7/8), 1221–1236.

Peterhans, E. and von der Heydt, R. (1989). Mechanisms of contour perception in monkey visual cortex II. Contours bridging gaps. *Journal of Neuroscience*, **9**(5), 1749–1763.

Pollen, D.A., Gaska, J.P., and Jacobsen, L.D. (1989). Physiological constraints on models of visual cortical function. In R.M.J. Cotterill (Ed.), **Models of brain function**. Cambridge: Cambridge University Press, pp. 115–135.

Prazdny, K. (1984). On the perception of glass patterns. *Perception*, **13**, 469–478.

Prinzmetal, W. (1990). Neon colors illuminate reading units. *Journal of Experimental Psychology: Human Perception and Performance*, **16**(3), 584–597.

Prinzmetal, W. and Boaz, K. (1989). Functional theory of illusory conjunctions and neon colors. *Journal of Experimental Psychology: General*, **118**(2), 165–190.

Ramachandran, V.S. (1981). **Perception of apparent movement: Studies in cognitive sciences, Volume II.** Irvine: University of California School of Social Sciences.

Ramachandran, V.S. and Inada, V. (1985). Spatial phase and frequency in motion capture of random-dot patterns. *Spatial Vision*, **1**, 57–67.

Shapley, R. and Gordon, J. (1985). Nonlinearity in the perception of form. *Perception and Psychophysics*, **37**, 84–88.

Snowden, R.J. (1989). Motions in orthogonal directions are mutually suppressive. *Journal of the Optical Society of America*, **6**(7), 1096–1101.

Snowden, R.J. (1990). Suppressive interactions between moving patterns: Role of velocity. *Perception and Psychophysics*, **47**(1), 74–78.

Sutter, A., Beck, J., and Graham, M. (1989). Contrast and spatial variables in texture segregation: Testing a simple spatial-frequency channels model. *Perception and Psychophysics*, **46**(4), 312–332.

Tanaka, M., Lee, B.B., and Creutzfeldt, O.D. (1983). Spectral tuning and contour representation in area 17 of the awake monkey. In J. D. Mollon and L. T. Sharpe (Eds.), **Colour vision**. New York: Academic Press.

Todd, J.T. and Akerstrom, R.A. (1987). Perception of three-dimensional form from patterns of optical texture. *Journal of Experimental Psychology: Human Perception and Performance*, **13**(2), 242–255.

von der Heydt, R., Hänny, P., and Dürsteler, M.R. (1981). The role of orientation disparity in stereoscopic perception and the development of binocular correspondence. In E. Grastyán and P. Molnár (Eds.), **Advances in physiological sciences, volume 16: Sensory functions**. Elmsford, NY: Pergamon Press.

von der Heydt, R., Peterhans, E., and Baumgartner, G. (1984). Illusory contours and cortical neuron responses. *Science*, **224**, 1260–1262.

Wallach, H. (1976). **On perception**. New York: Quadrangle/The New York Times Book Company.

Watanabe, T. and Sato, T. (1989). Effects of luminance contrast on color spreading and illusory contour in the neon color spreading effect. *Perception and Psychophysics*, **45**(4), 427–430.

Watanabe, T. and Takeichi, H. (1990). The relation between color spreading and illusory contours. *Perception and Psychophysics*, **47**(5), 457–467.

Watson, A.B. and Ahumada, A.J. (1985). Model of human visual-motion sensing. *Journal of the Optical Society of America A*, **2**, 322–342.

Welch, L. (1989). The perception of moving plaids reveals two motion-processing stages. *Nature* **337**, 734–736.

Williams, D. and Phillips, G. (1987). Cooperative phenomena in the perception of motion direction. *Journal of the Optical Society of America A*, **4**(5), 878–885.

Williams, D. and Sekuler, R. (1984). Coherent global motion percepts from stochastic local motions. *Vision Research*, **24**, 55–62.

Wilson, H.R. (1991). A psychophysically motivated model for two-dimensional motion perception. *Investigative Ophthalmology and Visual Science*, **32**(4), 893. Abstract #1101.

Zeki, S.M. (1974a). Functional organization of a visual area in the posterior bank of the superior temporal sulcus of the rhesus monkey. *Journal of Physiology (London)*, **236**, 549–573.

Zeki, S.M. (1974b). Cells responding to changing image size and disparity in the cortex of the rhesus monkey. *Journal of Physiology (London)*, **242**, 827–841.